Two decades of inorganic carbon dynamics along the Western Antarctic Peninsula

Claudine Hauri[1,2], Scott C. Doney[3], Taro Takahashi[4], Matthew Erickson[5], Grant Jiang[6], and Hugh W. Ducklow[4]

[1] International Pacific Research Center, SOEST, University of Hawai'i, Honolulu, HI, USA.
[2] International Arctic Research Center, University of Alaska Fairbanks, Fairbanks, AK, USA.
[3] Marine Chemistry and Geochemistry Department, Woods Hole Oceanographic Institution, Woods Hole, MA, USA.
[4] Lamont-Doherty Earth Observatory, Columbia University, Palisades, NY, USA.
[5] Antarctic Support Contractor, Arlington, VA, USA.
[6] School of Earth Sciences, University of Melbourne, Melbourne, VIC, Australia.

Correspondence to: C. Hauri (chauri@hawaii.edu)

Keywords: Southern Ocean, carbon dioxide, ocean acidification, climate change, trend, Redfield ratio

Abstract

We present 20 years of seawater inorganic carbon measurements collected along the western shelf and slope of the Antarctic Peninsula. Water column observations from summertime cruises and seasonal surface underway pCO_2 measurements provide unique insights into the spatial, seasonal and interannual variability of this dynamic system. Discrete measurements from depths >2000 m align well with World Ocean Circulation Experiment observations across the time-series and underline the consistency of the data set. Surface total alkalinity and dissolved inorganic carbon data showed large spatial gradients, with a concomitant wide range of Ω_{arag} (< 1 up to 3.9). This spatial variability was mainly driven by increasing influence of biological productivity towards the southern end of the sampling grid and melt water input along the coast towards the northern end. Large inorganic carbon drawdown through biological production in summer caused high near-shore Ω_{arag} despite glacial and sea-ice melt water input. In support of previous studies, we observed Redfield behavior of regional C/N nutrient utilization, while the C/P (80.5 ± 2.5) and N/P (11.7 ± 0.3) molar ratios were significantly lower than the Redfield elemental stoichiometric values. Seasonal salinity-based predictions of Ω_{arag} suggest that surface waters remained mostly supersaturated with regard to aragonite throughout the study. However, more than 20 % of the predictions for winters and springs between 1999 and 2013 resulted in $\Omega_{arag} < 1.2$. Such low levels of Ω_{arag} may have implications for important organisms such as pteropods. Even though we did not detect any statistically significant long-term trends, the combination of ongoing ocean acidification and freshwater input may soon induce more unfavorable conditions than the ecosystem experiences today.

1 Introduction

Antarctic continental shelves are viewed as strong anthropogenic CO_2 sinks and therefore play an important role in global biogeochemical cycles [*Arrigo et al.*, 2008]. These highly productive regions also support ecosystems that are exposed to rapid environmental change [*Ducklow et al.*, 2007, 2012]. Conditions along the western shelf of the Antarctic Peninsula (WAP, Figure 1) are characterized by rapid ocean-atmosphere warming, sea-ice retreat and melting of glaciers [*Ducklow et al.*, 2012; *Stammerjohn et al.*, 2012; *Meredith et al.*, 2013], impacting phytoplankton concentrations [*Montes-Hugo et al.*, 2009] and higher trophic level organisms such as krill, fish, and Adèlie Penguins [*Ducklow et al.*, 2007, 2012; *Schofield et al.*, 2010]. Climate and oceanographic trends are also mirrored in the inorganic carbon dynamics, which could feed back to global carbon cycling and/or enhance the projected fast progression of Southern Ocean acidification [*McNeil and Matear*, 2008; *Steinacher et al.*, 2009; *Bopp et al.*, 2013], thereby imposing additional environmental stressors on the ecosystem.

In the WAP, carbon biogeochemistry is controlled by an interplay of physical and biological mechanisms, which include photosynthesis, respiration, freshwater input, gas exchange, sea-ice cover, winds, and horizontal advection [*Carrillo and Karl*, 1999; *Carrillo et al.*, 2004; *Wang et al.*, 2009; *Montes-Hugo et al.*, 2010]. The physical oceanography of the region is strongly influenced by equatorward flow at the continental shelf/slope break associated with the eastward flowing Antarctic Circumpolar Current that abuts the continental slope along the WAP region. On the shelf, there are indications of one or more cyclonic circulation cells with poleward flow inshore [*Hofmann et al.,* 1996; *Dinniman and Klinck,* 2004; *Martinson et al.,* 2008]. Water mass properties are strongly influenced by subsurface intrusions onto the continental shelf of warm, nutrient and DIC rich Upper Circumpolar Deep Water (UCDW), that appears to be modulated by topographic depressions and canyons [*Martinson et al.* 2008; *Dinniman et al.,* 2011; *Martinson and McKee,* 2012]. In winter, respiration processes and the entrained deep CO_2-rich water increase the DIC concentration in surface waters to supersaturated levels of CO_2 with respect to the atmosphere [*Carrillo et al.*, 2004; *Wang et al.*, 2009; *Tortell et al.*, 2014; *Legge et al.,* 2015]. From austral spring through summer, sea-ice retreats from north to south and from offshore to inshore [*Smith and Stammerjohn*, 2001]. If not

79 counteracted by strong winds, freshwater from melting sea-ice, glaciers and snow
80 [*Meredith et al.*, 2013] stabilizes the water column in close proximity to the inshore and
81 southward moving sea-ice edge. Stratification and presumably iron availability provide
82 favorable conditions for phytoplankton blooms [*Garibotti et al.*, 2003, 2005; *Vernet et*
83 *al.*, 2008], resulting in a strong drawdown of dissolved inorganic carbon (DIC) and flux
84 of CO_2 from the atmosphere into the ocean [*Carrillo et al.*, 2004; *Montes-Hugo et al.*,
85 2009; *Wang et al.*, 2009]. Subsequent iron depletion results in a decreasing trend of
86 chlorophyll *a* (Chl *a*) from onshore to offshore, with interannual differences in the
87 gradient strength, depending on the onset of the sea-ice retreat [*Garibotti*, 2005; *Garibotti*
88 *et al.*, 2005], but possibly also the timing of sampling in relation to the timing of sea ice
89 retreat and phytoplankton blooms.
90 The inorganic carbon dynamics are further complicated by large-scale
91 atmospheric patterns. The El Niño Southern Oscillation (ENSO) and Southern Annular
92 Mode (SAM) drive the WAP climate and oceanography on interannual to multidecadal
93 timescales [*Yuan and Martinson*, 2001; *Stammerjohn et al.*, 2008a]. During La Niña
94 years, storms become longer and more intense, temperatures increase and sea ice extent
95 decreases in the WAP region as a result of a strong low-pressure system driven by the
96 poleward displacement of the polar jet [*Yuan*, 2004]. Positive SAM phases are also
97 associated with positive temperature anomalies over the Antarctic Peninsula and
98 decreased sea-ice extent [*Kwok*, 2002; *Stammerjohn et al.*, 2008]. Furthermore, the SAM
99 brings the Southern Hemisphere westerly winds closer to Antarctica, which amplifies the
100 typical features of La Niña. During these periods, nutrient and CO_2-rich Circumpolar
101 Deep Water intrudes more frequently on to the shelf [*Martinson et al.*, 2008], potentially
102 increasing [CO_2] on the shelf. On the other hand, weaker and fewer storms and spatial
103 and temporal extension of sea-ice coverage are observed in negative phases of SAM, with
104 associated stronger stratification of the water column and enhanced biological
105 productivity [*Saba et al.*, 2014]. These features are further intensified when a negative
106 SAM coincides with El Niño [*Stammerjohn et al.*, 2008b].
107 The WAP oceanography and ecosystem have been intensely observed as part of
108 the PAL-LTER (Palmer Long Term Ecological Research) program
109 (http://pal.lternet.edu/) over the past two decades [*Ducklow et al.*, 2007, 2012]. Since

1993, this multifaceted data set also contains seawater inorganic carbon measurements taken each January along transects shown in Figure 1. We complement the summertime inorganic carbon measurements from PAL-LTER with surface underway pCO_2 measurements that cover all four seasons [*Takahashi et al.*, 2015]. Here, we describe the spatial, seasonal and interannual variability of the inorganic carbon system over the past two decades with the intention to improve our understanding of the main physical and biological controls. Furthermore, such a uniquely long data set allows us to gain first insights into the impacts of ocean acidification on the region.

2 Data and Methods

2.1 In situ data and calculation of carbonate system variables

We used discrete measurements of seawater DIC, total alkalinity (TA) and nutrients collected during ship-based cruises as part of the PAL-LTER program, along with temperature and salinity from CTD casts. The data were gathered along the PAL-LTER sampling grid (Figure 1), which runs 500 km along the coast and 250 km across the shelf. The along shelf transects were spaced every 100 km, with 20 km between the stations. The data were collected on an annual summertime cruise each January - February from 1993 through 2012. Carbon system sample collection and analysis were performed by David Karl and Chris Carrillo for data prior to 2003, and by Hugh Ducklow and Matthew Erickson for data from 2003 onward, with the exception that DIC analysis was done by Taro Takahashi in 2003 and 2004. No TA data were collected during 2003-2004.

Following the WOCE-JGOFS protocols, discrete samples of DIC and TA (300 ml) from Niskin bottle casts were preserved with 200 µl saturated $HgCl_2$ solution and sealed [*Dickson and Goyet*, 1994]. DIC was analyzed by coulometric determination of extracted CO_2 [*Johnson et al.*, 1987]. TA was measured with the potentiometric titration method. Certified Reference Materials (provided by A.G. Dickson, Scripps Institution of Oceanography) were used to assure internal consistency of data with a precision of ± 2 µmol kg^{-1} for DIC and ± 5 µmol kg^{-1} for TA. Water for inorganic nutrient analysis was subsampled from Niskin bottles into acid washed 50 mL Falcon tubes and frozen at -70 °C. The samples were first analyzed using a Lachat Quickchem 8000 autoanalyzer at the University of California at Santa Barbara Marine Science Institute Analytical Lab (1993-

2007) and later at the Marine Biological Laboratory (Woods Hole MA, 2008 – 2012). Inorganic nutrient data reach a precision of ± 1 %. All PAL-LTER data and a detailed description of the sampling methodology are publicly available at http://pal.lternet.edu/ (dissolved inorganic nutrients, PAL-LTER dataset 27).

Calculated pH and saturation state for aragonite (Ω_{arag}) were determined from DIC, TA, temperature, salinity, phosphate, silicate and pressure using the CO2SYS MATLAB-version [*van Heuven et al.*, 2011]. To determine the carbonate variables we applied the dissociation constants for carbonic acid by *Dickson and Millero*, [1987] (refit from *Mehrbach et al.*, [1973]). The CO_2 solubility equations of *Weiss*, [1974], and dissociation constants for boric acid by *Dickson*, [1990] were also used to determine pH and Ω_{arag}. pH is reported on the total H^+ ion concentration scale (pHT).

The Lamont-Doherty Earth Observatory (LDEO) measured underway-surface pCO_2 with a precision of ± 0.5 %, together with salinity and temperature in various seasons between 1999 and 2013, using a shower-type water-gas equilibrator and infrared CO_2 gas analyzer (see www.ldeo.columbia.edu/pi/CO2 for the operational and engineering details [*Takahashi et al.*, 2015]). A range of five standard gas mixtures spanning between 100 ppm and 700 ppm mole fraction CO_2 certified by the Earth System Research Laboratory of the National Oceanic and Atmospheric Administration (NOAA) was used to calibrate the system every four hours.

2.2 Comparison with deep-water WOCE/CLIVAR inorganic carbon system data

We checked the consistency of the PAL-LTER DIC and TA data by comparing PAL-LTER deep-water (> 2000 m), offshore TA and DIC measurements to deep-water data collected during the World Ocean Circulation Experiment (WOCE) and Climate and Ocean – Variability, Predictability, and Change (CLIVAR) cruises along parts of sections A21 and S4P that were overlapping with the PAL-LTER grid (data available at http://www.nodc.noaa.gov/woce/wdiu/). The WOCE and CLIVAR shipboard measurements were calibrated using seawater certified reference materials (prepared by A. G. Dickson, Scripps Institute of Oceanography), leading to an estimated precision of ±2 μmol kg^{-1}. DIC was measured on all cruises. When necessary, TA was calculated from DIC and either fCO_2 or pCO_2 following the same procedure as described in Section

2.1. Figure 2a shows the stations along the WAP where deep-water samples were taken during PAL-LTER and WOCE cruises. PAL-LTER DIC and TA measurements were within the range of sampled/calculated DIC and TA from the WOCE and CLIVAR cruises, (Figures 2b and c). After removing five outliers, mean deep-water DIC (DIC^{mean} = 2260.6 ± 3.8 μmol kg^{-1}) and TA (TA^{mean} = 2365.4 ± 7.0 μmol kg^{-1}) from PAL-LTER cruises corresponded well with the data measured/calculated from WOCE cruises (DIC^{mean} = 2261.8 ± 3.0 μmol kg^{-1}; TA^{mean} = 2365.9 ± 9.3 μmol kg^{-1}).

2.3 Comparison with underway-surface pCO_2 data

We also undertook a quality check of the PAL-LTER discrete surface DIC and TA data (depth < 5 m) by comparing PAL-LTER pCO_2, which was calculated using observed DIC and TA values, to LDEO pCO_2. LDEO pCO_2 samples that were collected during the PAL-LTER cruises were spatially matched with the PAL-LTER derived pCO_2 values by choosing the nearest latitude and longitude pair within a 1 km distance. Four PAL-LTER pCO_2 outliers that underestimate/overestimate pCO_2 relative to the underway observations by more than 150 μatm were removed. Analysis of the corrected data set with a Linear Regression Type II model suggests a correlation of r = 0.82 (Figure A1, Table 1). Some of the observed discrepancies may be attributed to errors in matching the times of bottle samples with those of underway pCO_2 measurements. Seawater inorganic carbon chemistry is highly variable along the WAP due to the influence of productivity, respiration, freshwater and upwelling of CO_2-rich subsurface water [*Carrillo et al.*, 2004]. Small matching errors may therefore introduce small DIC and TA offsets, which would translate into larger fractional differences in pCO_2 due to the large Revelle Factor ($\partial \ln pCO_2 / \partial \ln DIC$) common in the region [*Sarmiento and Gruber*, 2006].

3 Results

Here, we examine the observed spatial summer patterns of DIC, TA, pHT and Ω_{arag} along the WAP and explore the underlying biological and physical drivers. We then discuss regional carbon – nutrient drawdown ratios and present our seasonal Ω_{arag} predictions that give initial insights into the chemical environment in the more poorly sampled spring, fall

and winter months. Finally, using the LTER and LDEO data sets, we investigate temporal trends over the past two decades.

3.1 Spatial summertime patterns of the inorganic carbon system

Surface waters in the PAL-LTER region exhibited high spatial and interannual variability of DIC (min = 1850 μmol kg^{-1} and max = 2173 μmol kg^{-1}), TA (min = 2087 μmol kg^{-1} and max = 2396 μmol kg^{-1}), and salinity (min = 30.3 and max = 33.9) across the shelf. As a result, surface Ω_{arag} reached levels as low as 0.98 in 1996, while maximum Ω_{arag} values were > 3 in several years (Figure 3). Off-shore, DIC (min = 2072 μmol kg^{-1} and max = 2255 μmol kg^{-1}), TA (2265 μmol kg^{-1} and 2355 μmol kg^{-1}), and salinity (min = 33.4 and max = 34) were less variable, resulting in a smaller Ω_{arag} range (min = 1.14 and max = 2.41). Additional aragonite undersaturation was detected between 100 and 200 m depth in 2005 and 2007 (Figure 3). At depths > 70 m, which is below the mixed layer depth, Ω_{arag} was < 1.5 in all years.

To gain a spatial overview of the general summertime surface features (upper 5 m), we linearly interpolated the observations in space and averaged across years with available DIC and TA (or nutrient) measurements. Averages are only shown for regions where samples were taken in more than 5 years (Figure 4). The resulting pCO_2, pHT, Ω_{arag}, TA, salinity, DIC, and nutrient fields exhibited clear onshore – offshore gradients. With the exception of DIC, all variables also followed a north-south gradient. Mean summertime surface pCO_2 was lowest (<200 μatm) in the southern coastal region and was about 60 to 70 μatm lower than in the northern near-shore regions (Figure 4a). The highest mean summertime pCO_2 values were found in the northern slope region (300-325 μatm). The opposite pattern was reflected in Ω_{arag} and pHT, with highest values (Ω_{arag}^{max} = 2.6 and pHT^{max} 8.3) close to the coast and south of 66.5°S (Figures 3b and c), decreasing along the coast towards the north to pHT ~8.2 and Ω_{arag} ~1.9, and reaching the lowest levels in northern offshore waters (pHT^{min} = 8.1; Ω_{arag}^{min} = 1.7). TA also exhibited north-south and onshore – offshore gradients, with values as low as 2185 μmol kg^{-1} in the northern near-shore regions and as high as > 2300 μmol kg^{-1} offshore. The low TA values along the northern part of the coast coincided with the lowest salinity values of 31.8, suggesting dilution of TA due to freshwater input (Figures 3d and e). Higher TA

values offshore were also reflected in increased DIC and salinity concentrations, with temperatures between 1.3 – 1.5 °C. DIC also exhibited an onshore–offshore gradient with values about 80 to 100 μmol kg^{-1} lower in the near shore region compared to offshore, but there was no significant north-south gradient despite the presence of freshwater in the north (Figure 4f). Salinity normalized DIC (sDIC, normalized with UCDW salinity = 34.7) was lowest in the southern region, thereby indicating that biological processes likely counteracted the expected north-south DIC gradient due to the pronounced freshwater influence on DIC in the north (Figure 4g).

3.2 Physical and biological drivers of the inorganic carbon system

In this section we examine the physical and biological mechanisms that control the observed variability in DIC and TA. DIC can decrease (increase) through dilution with freshwater (evaporation), organic matter production (remineralization), CO_2 outgassing to the atmosphere (CO_2 uptake) and/or precipitation of $CaCO_3$ (dissolution). While positive net community production decreases DIC, the biological effect of organic matter production on TA depends on the source of nitrogen, where nitrate consumption increases TA and ammonium consumption decreases TA [*Goldman and Brewer*, 1980]. Since nitrate is more abundant than ammonium in WAP surface waters [Serebrennikova and Fanning, 2004], nitrate was assumed as the nitrogen source. With a Redfield stoichiometry of 6.6 mol C/mol N then TA should increase by 1/6.6 = +0.15 μmol TA per μmol DIC consumed. Precipitation of biological $CaCO_3$ material reduces both DIC and TA with the effect on TA twice as large as that on DIC (2 μmol /μmol). TA is not affected by gas exchange but does vary as a result of dilution and evaporation.

Indications of surface reductions in TA and DIC due to freshwater input are evident along the WAP, and therefore freshwater processes (sea-ice and glacial melt, precipitation) [*Meredith et al.*, 2013] appear to be important factors influencing the summertime carbon dynamics along the WAP. Figure 5 shows TA (circles) and DIC (diamonds) as a function of salinity. The black lines represent the dilution lines for TA and DIC, which were calculated following *Yamamoto-Kawai et al.*, [2009]. UCDW end members are based on average TA and DIC concentrations in the water mass identified as

UCDW (black frames) [*Martinson et al.*, 2008]. Upper-ocean TA follows its dilution line closely, with stronger positive deviations of about 35 μmol kg^{-1} on average. In contrast, DIC values fall considerably below the dilution line. A DIC drawdown of about 60 μmol kg^{-1} is visible in the winter water (grey diamonds), which increased to more than 200 μmol kg^{-1} in the mixed layer, leading to Ω_{arag} as low as 1.5 and as high as 3.9.

The DIC drawdown relative to the salinity mixing-dilution line is most likely due to biological production of organic matter. Figure 6 shows sDIC as a function of salinity-normalized TA (sTA) for waters shallower than UCDW (orange dots). The regression line (solid black line, sTA = -0.11 x sDIC + 2601, RMSE = 18.6) ± 2σ (dashed lines) for estimated measurement precision (σ = +/- 5 μmol kg^{-1}) is similar to the nitrate-based photosynthesis line (blue line), indicating that the large decrease in DIC with the concomitant smaller increase in TA was mainly due to net biological production of organic matter. The photosynthesis line is based on winter water (WW) DIC and TA end-members (blue dots) and a slope of -1/6.2. According to the Redfield ratios (C/N/P = 106:16:1, [*Redfield*, 1958]), photosynthetic utilization of 1 mole of NO_3 increases TA by 1 μmol kg^{-1} [*Wolf-Gladrow et al.*, 2007] and decreases DIC by 106/16 (6.6). However, since the TA titration was performed to a pHT of about 3, the TA values include residual PO_4^{-3}, which leads to this slightly shallower slope of 6.2.

The intense, biologically driven DIC drawdown and resulting pCO_2 undersaturation in the mixed layer may have led to some CO_2 uptake from the atmosphere that tends to reduce the apparent DIC deficit; thus the estimated biological drawdown from observed DIC values in Figure 6 may be underestimated and needs to be corrected for air-sea CO_2 gas exchange from the period of biological drawdown to the sampling time. To account for DIC concentration changes due to gas exchange with the atmosphere, we assumed a constant atmospheric concentration of 390 μatm between 1993 and 2012, and a gas transfer rate (k) of 5 (±1) milli-mol CO_2 m^{-2} μatm^{-1} $month^{-1}$, which is the estimated mean rate for the Southern Ocean area south of 62 °S [Takahashi et al. 2009]. The change in DIC (μmol kg^{-1} $month^{-1}$) due to gas transfer into the mixed layer (ML) of d meters depth is:

$$\Delta DIC = k * \Delta t * \Delta pCO_2 / d.$$

ΔpCO_2 (pCO_2^{atm} - pCO_2^{ML}) was between -143 µatm and 312 µatm, as pCO_2^{ML} ranged from 533 µatm to 78 µatm, indicating that there was potential for both oceanic CO_2 uptake and outgassing. Assuming that d = 50 m [*Ducklow et al.*, 2013], we estimate that the monthly ΔDIC due to air-to-sea CO_2 gas exchange was in the range of -14 to 31 µmol kg^{-1} $month^{-1}$. Since the first large phytoplankton blooms generally occur after the sea-ice retreats in November (Δt ~3 months), we assume that by the time of sampling at the end of January, ΔDIC would fall in the range -43 to 94 µmol kg^{-1}. The DIC corrected for gas exchange is illustrated as grey dots in Figure 6. While applying the gas exchange correction flattens the regression line (grey line) somewhat, the photosynthesis line (blue) still remains within the estimated error bounds of the gas exchange corrected regression line (grey dotted lines), further emphasizing that photosynthesis is the key biological driver of the summertime carbonate system west of the Antarctic Peninsula.

3.3 Nutrient vs. carbon drawdown

Ocean carbon, nitrogen and phosphorus cycles are governed by organic matter production and subsequent remineralization and are strongly correlated on a global average with the proportions C/N/P = 106:16:1 [*Redfield*, 1958]. Our findings suggest that the carbon-nutrient cycles along the WAP depart from the standard Redfield values (Figure 7). In a few samples, the standing stock of PO_4^{3-} became depleted before NO_3^-, and overall the regression indicates a low N:P ratio of 9.8 ± 0.4 in the mixed layer (Figure 7a, black) and N:P = 11.7 ± 0.3 for all data (dark grey) relative to the standard Redfield value of 16 molN/mol P. The mole/mole C:P ratio was also considerably smaller than the Redfield ratio (Figure 7b). C:P yielded 43.1 ± 2.3 in the mixed layer and 55.0 ± 1.7 for all data. However, after applying the gas exchange correction on DIC (see section 3.2), the C:P ratio shifted closer to the Redfield Ratio and resulted in a value of 80.5 ± 2.5 (light grey dots and lines). Correcting the DIC for gas exchange shifted the molar ratio from 4.5 ± 0.2 (mixed layer depth) and 4.7 ± 0.1 (all data) to 6.7 ± 0.2 and resulted in a Redfield-like C:N ratio.

3.4 Seasonal variability

323 To get insights into the carbon dynamics during winter, spring, and fall, when direct
324 measurements of DIC, TA and nutrients are either scarce or not available, we developed a
325 regional TA algorithm (based on PAL-LTER summertime data). In combination with
326 seasonal LDEO pCO_2, salinity and temperature data, we calculated Ω_{arag} for the missing
327 seasons. Due to the weak correlation between PAL-LTER temperature and TA (r = 0.50),
328 we based the TA algorithm on salinity only (Figure A2, r = 0.88). Applying the Akaike
329 information criterion [*Burnham and Anderson*, 2002], we determined that TA along the
330 WAP will be best represented by a first order linear model. We then randomly divided
331 the PAL-LTER surface measurements (depth <5 m) into 10 data subsets using the 10-fold
332 cross validation method [*Stone*, 1974; *Breiman*, 1996]. Using 9 of the ten data sets we
333 derived a regression model, predicted the TA with the model, and calculated the model
334 coefficients and root mean square errors (RMSE). We repeated these steps so every data
335 subset was left out once. The coefficients for the final model were calculated from the
336 mean of the ten regression coefficients. We found the best fit in the following equation:

337 $$TA^{pred}\ (\mu mol\ kg^{-1}) = 57.01\ (\pm\ 0.88)\ x\ S + 373.86\ (\pm\ 35.26),$$

338 which resulted in a linear correlation coefficient of r = 0.88 and a RMSE of 15.2 μmol
339 kg^{-1} (Figure A2). In combination with the pCO_2 measurement precision of 3 μatm, the
340 RMSE of TA prediction resulted in a mean error in calculated Ω_{arag} of 0.0219 units and
341 pHT of 0.0043 [*Glover et al.*, 2011]. Note that the calculated Ω_{arag} and pHT estimates
342 implicitly require that the approximately linear summertime TA-salinity relationship
343 holds for the other seasons, a reasonable assumption if dilution and mixing substantially
344 affect TA patterns.

345 Summertime LDEO underway pCO_2 values were, on average, lower than during
346 the rest of the year (Figure 8a). While only a small percentage of these summertime
347 values reached levels higher than the atmospheric CO_2 concentration, 70 % of the water
348 samples taken in winter were supersaturated with regard to atmospheric CO_2 (>390
349 μatm). Spring and fall pCO_2 values were also generally higher than summertime
350 measurements and ranged from 207 to 506 μatm and 90 to 414 μatm.

351 Our salinity-based algorithm predicted the majority of all TA ranging between
352 2200 and 2300 μmol kg^{-1} in all seasons, with the most frequent occurrence of highest TA

353 in winter and spring (Figure 8b). Some summertime TA was predicted to be as low as
354 2056 μmol kg^{-1}.

355 Prediction of seasonal Ω_{arag} revealed that surface waters of the WAP were
356 supersaturated with regard to aragonite throughout the years (Figure 8c). The most
357 frequent occurrence of low Ω_{arag} was in winter and spring, when most of the predicted
358 values resulted in $\Omega_{arag} < 1.4$. 20 % of spring and winter values were $\Omega_{arag} < 1.2$, with the
359 lowest predicted surface Ω_{arag} reaching near aragonite undersaturation in winter. Similar
360 to the LTER observations, predicted summertime Ω_{arag} displayed a large range, spanning
361 from 1.1 to 4.1, with the majority of predictions between 1.3 and 1.8. Biological
362 production in summer is sufficiently intense to prevent low Ω_{arag} values during the active
363 growing season when its effects might be most pronounced.
364
365 **3.5 Temporal trends**
366 Trend analysis of the PAL-LTER data showed no statistically significant annual trends
367 (at the 95% confidence level) in the measured carbon parameters, temperature or salinity
368 in surface waters in summer between 1993 and 2012 (Table 2). As a comparison, we
369 conducted a trend analysis for the LDEO surface underway pCO_2 data set (1999 – 2013)
370 in the same region. LDEO observations show an increasing, but not statistically
371 significant trend in surface pCO_2, supporting our results above (Table 3). The largest
372 increasing trend was found in fall, (1.9 ± 0.95 μatm yr^{-1}), but this trend was also slightly
373 outside the confidence interval and therefore statistically not significant.
374
375 **4 Discussion**
376 The 20 year-long PAL-LTER seawater inorganic carbon time-series showed a distinct
377 upper-ocean spatial pattern of onshore–offshore and north – south gradients and suggests
378 that the summertime carbon dynamics are primarily controlled by biological productivity
379 and freshwater input in near-shore areas.

380 Surface Ω_{arag} was distributed across a wide range (<1 to values > 3) in freshwater-
381 influenced areas with salinities $S < 32$ (Figure 5). To better understand how such a wide
382 range of Ω_{arag} at relatively low salinities was possible, we quantified the effect of
383 freshwater and biological production. Mixing of seawater with sea-ice or glacial

384 meltwater leads to a 'dilution' of CO_3^{2-} ions and a decrease in Ω_{arag} because TA and DIC
385 in glacial and sea-ice meltwater are much lower than in seawater [*Anderson et al.*, 2000;
386 *Yamamoto-Kawai et al.*, 2009]. Calculations of salinity normalized Ω_{arag} using sDIC and
387 sTA showed that freshwater input decreased Ω_{arag} by up to 0.2 units along the coast.
388 Despite the negative effect of freshwater on Ω_{arag}, the water in the south was nonetheless
389 highly supersaturated with $CaCO_3$. The salinity normalized DIC in the near-shore
390 southern region of the PAL-LTER sampling grid was up to 177 μmol kg^{-1} lower than
391 elsewhere, suggesting that near-shore phytoplankton blooms balanced out the negative
392 effect of freshwater on Ω_{arag} and even increased Ω_{arag} by up to 2 units. In 2005, when the
393 above-described pattern was particularly conspicuous, high Chl *a* (up to 20 μg/L) in the
394 southern coastal area of the sampling grid provides further evidence that high primary
395 productivity led to the observed high Ω_{arag} despite the presence of freshwater. Similar
396 results were found after the calving event of the Mertz glacier tongue in eastern
397 Antarctica, where enhanced primary productivity increased the Ω_{arag} and thereby
398 counteracted the effect of dilution by meltwater input [*Shadwick et al.*, 2013].
399 Our findings of onshore-offshore and latitudinal gradients of carbon parameters
400 are supported by previous results that suggest similar patterns for several physical and
401 biogeochemical parameters. Summertime surface temperature, salinity and $NO_3^- + NO_2^-$
402 are generally lower close to the coast, while Chl *a*, primary production, $Si(OH)_2$ and
403 water column stability decrease from the coast toward the open ocean [*Smith*, 2001;
404 *Garibotti et al.*, 2003; *Vernet et al.*, 2008]. The freshwater along the coast may originate,
405 to a large part, from melting of glacial ice and snow [*Meredith et al.*, 2013]. Such glacial
406 and snow-melt plumes have been correlated with increased primary production due to a
407 stabilization of the mixed layer, which creates favorable conditions for phytoplankton
408 blooms [*Dierssen et al.*, 2002]. This in turn is thought to be the dominant control of the
409 onshore-offshore gradient of phytoplankton variability and associated biologically-
410 impacted parameters. The north-south gradients possibly reflect the timing of
411 phytoplankton blooms in the north and south. As such, blooms in the north occur sooner
412 than blooms in the south [*Smith et al.*, 2008] – thus on average the PAL-LTER January
413 cruise takes place after the bloom in the north, and during the blooms in the south. This
414 may also be the reason for the nutrient depletion along the coast, despite low biological

productivity at the time of sampling in the north (Figure 4h and i). However, it is important to note that as a result of changes in ice cover, cloud formation and wind over the past 30 years, biological productivity has increased in the southern part of the WAP and significantly decreased north of 63°S [*Montes-Hugo et al.*, 2009]. The observed DIC drawdown in the winter water (Figure 5 and A3) may be a result of biological productivity, which is supported by previous observations of Chl *a* maxima in the euphotic part of the winter water, likely due to increased iron concentrations there [*Garibotti et al.*, 2003; *Garibotti*, 2005]. However, it is also likely that lateral advection or vertical mixing of low DIC water into the winter water have caused this signal.

Low Ω_{arag} values (< 1.35) observed offshore coincided with surface waters supersaturated with regard to atmospheric CO_2, salinities >33.5, and temperatures between 1.3 – 1.5 °C (not shown). These physical properties are associated with modified UCDW, a mixture between UCDW and Antarctic Surface Water [*Smith et al.*, 1999] and indicate that upwelling of DIC and TA rich water into the mixed layer may lead to lower Ω_{arag} conditions offshore [*Carrillo et al.*, 2004].

The PAL-LTER data indicate N:P uptake ratios lower than the Redfield ratio of 16:1, and uptake ratios similar to our findings (14:1) are common for the polar region of the Southern Ocean [*Weber and Deutsch*, 2010; *Martiny et al.*, 2013]. Our observed low ratio may be the result of a high abundance of diatoms with low N/P ratios in this cold and nutrient-rich environment [*Arrigo,* 1999; *Arrigo et al.,* 2002; *Green and Sambrotto*, 2006; *Martiny et al.*, 2013]. *Rubin et al.,* [1998] observed a similar N/P ratio of 13.0 ± 1.2 in the mixed layer south of the Polar Front, and an even lower N/P ratio of 11.3 ± 0.3 was observed in the iron-spiked mixed layer during the iron fertilization experiment in the Subantarctic South Pacific [*Hales and Takahashi*, 2012]. Consistent with the low N/P ratio, the observed C:P ratio (80.5 ± 2.5 ,corrected for gas exchange) was also lower than the classic Redfield ratio. This indicates that the regional phosphate cycle shows non-Redfield behavior, which is in agreement with the observed C:P ratio of 91.4 ± 7.9 in the mixed layer south of the Polar Front [*Rubin et al.*, 1998]. For the same region, *Rubin et al*., [1998] describe Redfield behavior of C/N nutrient utilization, which corresponds with our gas exchange corrected C/N nutrient utilization ratio of 6.7 ± 0.2. Recently published work suggests that C/N/P ratios exhibit a latitudinal pattern, with a range of 66:11:1 to

446 74:13:1 at higher latitudes in the Southern Ocean [*Martiny et al.*, 2013] and can therefore
447 be significantly lower than what we found in this study.
448 TA variability was largely driven by dilution through freshwater input and mixing
449 (Figure 5), which is well characterized by the salinity-derived TA relationship presented
450 in section 3.4. However, biological mechanisms such as photosynthesis, respiration,
451 $CaCO_3$ precipitation and dissolution also played an important role in controlling TA
452 concentrations in the water column and at the surface (Figure 6). Neglecting these
453 important drivers may be responsible for the large RMSE of our predicted TA (Figure
454 A2) relative to other studies that either had additional parameters at hand (i.e. O_2 or
455 nutrients) to derive inorganic carbon system parameters in coastal environments [*Juranek*
456 *et al.*, 2009; *Kim et al.*, 2010; *Evans et al.*, 2013] or that used salinity algorithms to
457 predict TA in open-ocean regions [*Takahashi et al.*, 2014]. Furthermore, TA varied by
458 more than 70 μmol kg^{-1} at salinities >33.7, which led to an unbalanced distribution of
459 residuals (Figure A2c). Increasing TA at higher salinities and nearly constant DIC
460 concentrations has been observed before in Arctic and Antarctic regions *[Dieckmann et*
461 *al., 2008; Fransson et al., 2011; Rysgaard et al., 2012; Shadwick et al., 2014; Legge et*
462 *al.,* 2015] and may be due to formation of ikaite crystals ($CaCO_3.6H_2O$) [*Suess et al.*,
463 1982] that store TA in sea-ice and, upon melting, release the excess TA into the surface
464 water [*Rysgaard et al.*, 2012, 2013]. However, reasons for the observed increasing TA at
465 higher salinities along the WAP remain speculative, since direct evidence of ikaite
466 formation/dissolution such as an increase in DIC associated with TA increase is missing
467 (Figure 6). A combination of other mechanisms, such as upwelling of high salinity –
468 high TA waters concomitant with biological DIC drawdown, could have increased
469 TA:DIC ratios at high salinities. Finally, the WAP region is very dynamic, with large
470 seasonal changes that may affect the carbon system in ways not representable by one
471 algorithm and may therefore require seasonally adjusted algorithms.
472 Despite of the above-described shortcomings in our salinity-derived TA
473 algorithm, the estimated Ω_{arag} values give a useful overview of the seasonal distribution
474 and variability of Ω_{arag} (Figure 8). Error propagation of pCO_2 measurement precision and
475 TA prediction accuracy suggests that the predicted error for Ω_{arag} may be as little as 0.02
476 [*Glover et al.*, 2011]. The seasonal estimations of Ω_{arag} suggest that some winter and

springtime Ω_{arag} were near Ω_{arag} = 1 and 20 % were between 1.0 and 1.2 (Figure 8). Short-term exposure to low levels of Ω_{arag} may cause severe dissolution of live pteropod shells and has already been observed in the Scotia Sea [*Bednaršek et al.*, 2012]. Surface aragonite undersaturation along the WAP may be a result of ocean acidification and may not have been common during preindustrial times [*Hauri et al.*, under review].

The large uncertainties in our estimated temporal trends are caused inherently by the large spatial and temporal variability of our data. Nevertheless, our mean rates of 1.45 ± 2.97 for summer and 0.43± 0.77 μatm yr^{-1} for winter suggest that the surface water pCO_2 has been increasing at a slower rate than the atmospheric pCO_2 rate of about 1.9 μatm yr^{-1}, and that the air-to-sea CO_2 driving potential has been increasing. Our results may be compared with the recent analysis of the 2002-2015 time-series data obtained across the Drake Passage by *Munro et al.* [in press]. In the waters south of the Polar Front (their Zone 4, closest to the LTER area), they observed that the surface water pCO_2 increased at a rate of 1.30 ± 0.85 μatm yr^{-1} in summer and 0.67 ± 0.39 μatm yr^{-1} in winter, which are comparable with ours along the WAP. We observed the strongest but still statistically insignificant increase in surface pCO_2 in fall (1.9 μatm $year^{-1}$, p = 0.0685). This increase corresponds with the mean atmospheric pCO_2 increase of 1.9 μatm per year, which causes a pHT decrease of about 0.02 per decade [*Takahashi et al.*, 2014]. Interestingly, *Stammerjohn et al.*, [2008a, 2008b] found that sea ice extent and wind are also changing most rapidly in spring and fall, which may enhance sea-air gas exchange and therefore facilitate positive pCO_2 trends. Furthermore, it is likely that the strong counter effect of biological productivity successfully masks the pCO_2 trend in summer, and decreased gas exchange due to sea ice weakens the trend in winter. However, the WAP climate and oceanography are regulated by large-scale atmospheric patterns, such as El Niño Southern Oscillation and Southern Annular Model [*Stammerjohn et al.*, 2008a], which may also influence the region's inorganic carbon chemistry on an interannual scale. A longer measurement period may be needed in order to be able to distinguish with certainty between natural variability and secular trends [*Henson et al.*, 2010].

5 Conclusions

This study gives new insights into the spatial and temporal variability of the WAP inorganic carbon system and its main physical and biological drivers. In particular, we found that large inorganic carbon drawdown through biological production in summer caused high near-shore Ω_{arag}, despite glacial and sea-ice melt water input. Furthermore, the data do not show a significant long-term trend in any of the inorganic carbon chemistry variables measured. Continuation and expansion of the inorganic carbon chemistry timeseries across other seasons is necessary to distinguish between natural variability and secular trends and to better understand synergistic effects of ocean acidification and climate change. Due to the region's physical complexity of circulation and forcing, and strong dynamic response to climate variability, we recommend development of a highly resolved biogeochemical model to complement our observational work. Implementation of modeling studies will improve our mechanistic understanding of how interannual variability and anthropogenic climate change impact the inorganic carbon chemistry along the WAP, which is imperative to predict the potential impact on the unique WAP ecosystem.

Author Contributions

Designed research: HD and TT. Field sampling and analytical measurements: TT, HD and ME. Data analysis and interpretation: CH with help from all co-authors. Wrote the paper: CH with help from SD, TT, and HD.

Acknowledgements

We thank past and present members of the Palmer LTER program as well as the captains and crew of the U.S. Antarctic research vessels. We are especially grateful to Richard Iannuzzi and James Conners for their support with data management, and to Tim Newberger for underway pCO_2 measurements. We gladly acknowledge support from the National Science Foundation Polar Programs (NSF OPP-90-11927, OPP-96-32763, OPP-02-17282, OPP-08-23101, and PLR-1440435). TT and the Ship of Opportunity Observation Program (SOOP) were supported by a grant (NA10OAR4320143) from the United States NOAA. This is International Pacific Research Center contribution number 1117.

References

Anderson, S. P., J. I. Drever, C. D. Frost, and P. Holden (2000), Chemical weathering in the foreland of a retreating glacier, *Geochim. Cosmochim. Acta*, *64*(7), 1173–1189, doi:10.1016/S0016-7037(99)00358-0.

544 Arrigo, K. R. (1999), Phytoplankton Community Structure and the Drawdown of
545 Nutrients and CO_2 in the Southern Ocean, *Science (80-.).*, *283*(5400), 365–367,
546 doi:10.1126/science.283.5400.365.

547 Arrigo, K. R. (2002), Taxon-specific differences in C/P and N/P drawdown for
548 phytoplankton in the Ross Sea, Antarctica, *Geophys. Res. Lett.*, *29*(19), 1938,
549 doi:10.1029/2002GL015277.

550 Arrigo, K. R., G. van Dijken, and S. Pabi (2008), Impact of a shrinking Arctic ice cover
551 on marine primary production, *Geophys. Res. Lett.*, *35*(19), L19603,
552 doi:10.1029/2008GL035028.

553 Bednaršek, N. et al. (2012), Extensive dissolution of live pteropods in the Southern
554 Ocean, *Nat. Geosci.*, *5*(12), 881–885, doi:10.1038/ngeo1635.

555 Bopp, L. et al. (2013), Multiple stressors of ocean ecosystems in the 21st century:
556 projections with CMIP5 models, *Biogeosciences*, *10*(10), 6225–6245,
557 doi:10.5194/bg-10-6225-2013.

558 Breiman, L. (1996), Stacked regressions, *Mach. Learn.*, *24*(1), 49–64,
559 doi:10.1007/BF00117832.

560 Burnham, K. P., and D. R. Anderson (2002), *Model selection and multimodel inference:*
561 *A practical information-theoretic approach*, Springer Verlag, New York.

562 Carrillo, C. J., and D. M. Karl (1999), Dissolved inorganic carbon pool dynamics in
563 northern Gerlache Strait, Antarctica, *J. Geophys. Res.*, *104*(C7), 15873,
564 doi:10.1029/1999JC900110.

565 Carrillo, C. J., R. C. Smith, and D. M. Karl (2004), Processes regulating oxygen and
566 carbon dioxide in surface waters west of the Antarctic Peninsula, *Mar. Chem.*, *84*(3-
567 4), 161–179, doi:10.1016/j.marchem.2003.07.004.

568 Dickson, A. G. (1990), Thermodynamics of the dissociation of boric acid in synthetic
569 seawater from 273.15 to 318.15 K, *Deep Sea Res. Part A. Oceanogr. Res. Pap.*,
570 *37*(5), 755–766, doi:10.1016/0198-0149(90)90004-F.

571 Dickson, A. G., and C. Goyet (1994), *Handbook of methods for the analysis of the*
572 *various parameters of the carbon dioxide system in sea water*, ORNL/CDIAC-74.

573 Dickson, A. G., and F. J. Millero (1987), A comparison of the equilibrium constants for
574 the dissociation of carbonic acid in seawater media, *Deep Sea Res. Part A.*
575 *Oceanogr. Res. Pap.*, *34*(10), 1733–1743, doi:10.1016/0198-0149(87)90021-5.

576 Dieckmann, G. S., G. Nehrke, S. Papadimitriou, J. Göttlicher, R. Steininger, H. Kennedy,
577 D. Wolf-Gladrow, and D. N. Thomas (2008), Calcium carbonate as ikaite crystals in
578 Antarctic sea ice, *Geophys. Res. Lett.*, *35*(8), L08501, doi:10.1029/2008GL033540.

579 Dierssen, H. M., R. C. Smith, and M. Vernet (2002), Glacial meltwater dynamics in
580 coastal waters west of the Antarctic peninsula., *Proc. Natl. Acad. Sci. U. S. A.*,
581 *99*(4), 1790–5, doi:10.1073/pnas.032206999.

582 Dinniman, M.S., and J.M. Klinck, 2004. A model study of circulation and cross-shelf
583 exchange on the west Antarctic Peninsula continental shelf, Deep-Sea Research II
584 51, 2003–2022
585
586 Dinniman, M.S., J.M. Klinck, W.O. Smith Jr. (2011) A model study of Circumpolar
587 Deep Water on the West Antarctic Peninsula and Ross Sea continental shelves, Deep
588 Sea Research Part II: Topical Studies in Oceanography, Volume 58, Issues 13–16,
589 July–August 2011, Pages 1508–1523

590 Ducklow, H. et al. (2013), West Antarctic Peninsula: An Ice-Dependent Coastal Marine
591 Ecosystem in Transition, *Oceanography*, *26*(3), 190–203,
592 doi:10.5670/oceanog.2013.62.

593 Ducklow, H. W., K. Baker, D. G. Martinson, L. B. Quetin, R. M. Ross, R. C. Smith, S. E.
594 Stammerjohn, M. Vernet, and W. Fraser (2007), Marine pelagic ecosystems: the
595 West Antarctic Peninsula, *Philos. Trans. R. Soc. B Biol. Sci.*, *362*(1477), 67–94,
596 doi:10.1098/rstb.2006.1955.

597 Ducklow, H. W. et al. (2012), The Marine System of the Western Antarctic Peninsula, in
598 *Antarctic Ecosystems: An Extreme Environment in a Changing World*, edited by A.
599 D. Rogers, N. M. Johnston, E. J. Murphy, and A. Clarke, John Wiley & Sons, Ltd.

600 Evans, W., J. T. Mathis, P. Winsor, H. Statscewich, and T. E. Whitledge (2013), A
601 regression modeling approach for studying carbonate system variability in the
602 northern Gulf of Alaska, *J. Geophys. Res. Ocean.*, *118*(1), 476–489,
603 doi:10.1029/2012JC008246.

604 Fransson, A., M. Chierici, P. L. Yager, and W. O. Smith (2011), Antarctic sea ice carbon
605 dioxide system and controls, *J. Geophys. Res.*, *116*(C12), C12035,
606 doi:10.1029/2010JC006844.

607 Garibotti, I., M. Vernet, M. Ferrario, R. Smith, R. Ross, and L. Quetin (2003),
608 Phytoplankton spatial distribution patterns along the western Antarctic Peninsula
609 (Southern Ocean), *Mar. Ecol. Prog. Ser.*, *261*, 21–39, doi:10.3354/meps261021.

610 Garibotti, I. A. (2005), Interannual variability in the distribution of the phytoplankton
611 standing stock across the seasonal sea-ice zone west of the Antarctic Peninsula, *J.*
612 *Plankton Res.*, *27*(8), 825–843, doi:10.1093/plankt/fbi056.

613 Garibotti, I. A., M. Vernet, and M. E. Ferrario (2005), Annually recurrent
614 phytoplanktonic assemblages during summer in the seasonal ice zone west of the
615 Antarctic Peninsula (Southern Ocean), *Deep Sea Res. Part I Oceanogr. Res. Pap.*,
616 *52*(10), 1823–1841, doi:10.1016/j.dsr.2005.05.003.

617 Glover, D., W. Jenkins, and S. Doney (2011), *Modeling methods for marine science*, 1st
618 ed., Cambridge University Press, New York.

619 Goldman, J., and P. G. Brewer (1980), Effect of nitrogen source and growth rate on
620 phytoplankton-mediated changes in alkalinity, *Limnol. Oceanogr.*, *25*(2), 352–357,
621 doi:10.4319/lo.1980.25.2.0352.

622 Green, S. E., and R. N. Sambrotto (2006), Plankton community structure and export of C,
623 N, P and Si in the Antarctic Circumpolar Current, *Deep Sea Res. Part II Top. Stud.*
624 *Oceanogr.*, *53*(5-7), 620–643, doi:10.1016/j.dsr2.2006.01.022.

625 Hales, B., and T. Takahashi (2012), Mesoscale biogeochemical responses to iron
626 fertilization in the upper layers of the Southern Ocean Iron Experiment areas, *J.*
627 *Geophys. Res.*, *117*(C1), C01018, doi:10.1029/2011JC006956.

628 Hauri, C., T. Friedrich, and A. Timmermann (under revision), Abrupt onset and
629 prolongation of aragonite undersaturation events in the Southern Ocean, *Nature*
630 *Climate Change*.

631 Henson, S. A., J. L. Sarmiento, J. P. Dunne, L. Bopp, I. Lima, S. C. Doney, J. John, and
632 C. Beaulieu (2010), Detection of anthropogenic climate change in satellite records
633 of ocean chlorophyll and productivity, *Biogeosciences*, *7*(2), 621–640,
634 doi:10.5194/bg-7-621-2010.

635 Hofmann, E.E., Klinck, J.M., Lascara, C.M., Smith, D.A., 1996. Water mass distribution
636 and circulation west of the Antarctic Peninsula and including Bransfield Strait. In:
637 Ross, Robin M., Hofmann, Eileen E., Quetin, Langdon B. (Eds.), Foundations for
638 Ecological Research West of the Antarctic Peninsula, Antarctic Research Series, vol.
639 70. American Geophysical Union, Washington, DC, pp. 61–80.

640 Van Heuven, S., D. Pierrot, J. W. B. Rae, E. Lewis, and D. W. R. Wallace (2011),
641 MATLAB Program Developed for CO2 System Calculations,

642 Johnson, K. ., J. M. Sieburth, P. J. le. Williams, and L. Brändström (1987), Coulometric
643 total carbon dioxide analysis for marine studies: Automation and calibration, *Mar.*
644 *Chem.*, *21*(2), 117–133, doi:10.1016/0304-4203(87)90033-8.

645 Juranek, L. W., R. A. Feely, W. T. Peterson, S. R. Alin, B. Hales, K. Lee, C. L. Sabine,
646 and J. Peterson (2009), A novel method for determination of aragonite saturation
647 state on the continental shelf of central Oregon using multi-parameter relationships

with hydrographic data, *Geophys. Res. Lett.*, *36*(24), L24601, doi:10.1029/2009GL040778.

Kim, T. W., K. Lee, R. A. Feely, C. L. Sabine, C. T. A. Chen, H. J. Jeong, and K. Y. Kim (2010), Prediction of Sea of Japan (East Sea) acidification over the past 40 years using a multiparameter regression model, *Global Biogeochem. Cycles*, *24*(3), doi:10.1029/2009GB003637.

Kwok, R. (2002), Spatial patterns of variability in Antarctic surface temperature: Connections to the Southern Hemisphere Annular Mode and the Southern Oscillation, *Geophys. Res. Lett.*, *29*(14), 1705, doi:10.1029/2002GL015415.

Legge, O. J., D. C. E. Bakker, M. T. Johnson, M. P. Meredith, H. J. Venables, P. J. Brown, and G. A. Lee, The seasonal cycle of ocean-atmosphere CO_2 flux in Ryder Bay, west Antarctic Peninsula, *Geophys. Res. Lett.*, 42, 2934-2942, doi:10.1002/2015GL063796.

Martinson, D. G., S. E. Stammerjohn, R. A. Iannuzzi, R. C. Smith, and M. Vernet (2008), Western Antarctic Peninsula physical oceanography and spatio–temporal variability, *Deep Sea Res. Part II Top. Stud. Oceanogr.*, *55*(18-19), 1964–1987, doi:10.1016/j.dsr2.2008.04.038.

Martinson DG, McKee DC (2012) Transport of warm Upper Circumpolar Deep Water onto the western Antarctic Peninsula continental shelf. Ocean Science 8:433-442

Martiny, A. C., C. T. A. Pham, F. W. Primeau, J. A. Vrugt, J. K. Moore, S. A. Levin, and M. W. Lomas (2013), Strong latitudinal patterns in the elemental ratios of marine plankton and organic matter, *Nat. Geosci.*, *6*(4), 279–283, doi:10.1038/ngeo1757.

McNeil, B. I., and R. J. Matear (2008), Southern Ocean acidification: a tipping point at 450-ppm atmospheric CO2., *Proc. Natl. Acad. Sci. U. S. A.*, *105*(48), 18860–4, doi:10.1073/pnas.0806318105.

Mehrbach, C., C. H. Culberson, J. E. Hawley, and R. M. Pytkowicz (1973), Measurement of the apparent dissociation constants of carbonic acid in seawater at atmospheric pressure, *Limnol. Oceanogr.*, *18*(6), 897–907, doi:10.4319/lo.1973.18.6.0897.

Meredith, M. P., H. J. Venables, A. Clarke, H. W. Ducklow, M. Erickson, M. J. Leng, J. T. M. Lenaerts, and M. R. van den Broeke (2013), The Freshwater System West of the Antarctic Peninsula: Spatial and Temporal Changes, *J. Clim.*, *26*(5), 1669–1684, doi:10.1175/JCLI-D-12-00246.1.

Montes-Hugo, M., S. C. Doney, H. W. Ducklow, W. Fraser, D. Martinson, S. E. Stammerjohn, and O. Schofield (2009), Recent changes in phytoplankton communities associated with rapid regional climate change along the western Antarctic Peninsula., *Science*, *323*(5920), 1470–3, doi:10.1126/science.1164533.

684 Montes-Hugo, M., C. Sweeney, S. C. Doney, H. Ducklow, R. Frouin, D. G. Martinson, S.
685 Stammerjohn, and O. Schofield (2010), Seasonal forcing of summer dissolved
686 inorganic carbon and chlorophyll a on the western shelf of the Antarctic Peninsula,
687 *J. Geophys. Res.*, *115*(C3), C03024, doi:10.1029/2009JC005267.

688 Munro, D. R., Lovenduski, N. S., Takahashi, T., Stephens, B. B, Newberger, T. and
689 Sweeney, C. (in press). A strengthening Southern Ocean CO_2 sink from Drake Passage
690 time-series observations. Geophys. Res. Letters., doi:10.1002/2015GL065194.

691 Redfield, A. (1958), The biological control of chemical factors in the environment, *Am.*
692 *Sci.*, *3*, 205–221.

693 Rubin, S. I., T. Takahashi, D. W. Chipman, and J. G. Goddard (1998), Primary
694 productivity and nutrient utilization ratios in the Pacific sector of the Southern
695 Ocean based on seasonal changes in seawater chemistry, *Deep Sea Res. Part I*
696 *Oceanogr. Res. Pap.*, *45*(8), 1211–1234, doi:10.1016/S0967-0637(98)00021-1.

697 Rysgaard, S., R. N. Glud, K. Lennert, M. Cooper, N. Halden, R. J. G. Leakey, F. C.
698 Hawthorne, and D. Barber (2012a), Ikaite crystals in melting sea ice – implications
699 for pCO_2 and pH levels in Arctic surface waters, *Cryosph.*, *6*(4), 901–908,
700 doi:10.5194/tc-6-901-2012.

701 Rysgaard, S. et al. (2013), Ikaite crystal distribution in winter sea ice and implications for
702 CO_2 system dynamics, *Cryosph.*, *7*(2), 707–718, doi:10.5194/tc-7-707-2013.

703 Saba, G. K. et al. (2014), Winter and spring controls on the summer food web of the
704 coastal West Antarctic Peninsula., *Nat. Commun.*, *5*, 4318,
705 doi:10.1038/ncomms5318.

706 Sarmiento, J. L., and N. Gruber (2006), *Ocean Biogeochemical Dynamics*, Princeton
707 University Press, Princeton, NJ.

708 Schofield, O., H. W. Ducklow, D. G. Martinson, M. P. Meredith, M. A Moline, and W.
709 R. Fraser (2010), How do polar marine ecosystems respond to rapid climate
710 change?, *Science*, *328*(5985), 1520–3, doi:10.1126/science.1185779.

711 Shadwick, E. H., S. R. Rintoul, B. Tilbrook, G. D. Williams, N. Young, A. D. Fraser, H.
712 Marchant, J. Smith, and T. Tamura (2013), Glacier tongue calving reduced dense
713 water formation and enhanced carbon uptake, *Geophys. Res. Lett.*, *40*(5), 904–909,
714 doi:10.1002/grl.50178.

715 Shadwick, E. H., B. Tilbrook, and G. D. Williams (2014), Carbonate chemistry in the
716 Mertz Polynya (East Antarctica): Biological and physical modification of dense
717 water outflows and the export of anthropogenic CO_2, *J. Geophys. Res. Ocean.*,
718 *119*(1), 1–14, doi:10.1002/2013JC009286.

719 Smith, D. A., E. E. Hofmann, J. M. Klinck, and C. M. Lascara (1999), Hydrography and
720 circulation of the West Antarctic Peninsula Continental Shelf, *Deep Sea Res. Part I*
721 *Oceanogr. Res. Pap.*, *46*(6), 925–949, doi:10.1016/S0967-0637(98)00103-4.

722 Smith, R. C. (2001), Variability of Primary Production in an Antarctic Marine Ecosystem
723 as Estimated Using a Multi-scale Sampling Strategy, *Integr. Comp. Biol.*, *41*(1), 40–
724 56, doi:10.1093/icb/41.1.40.

725 Smith, R. C., and S. E. Stammerjohn (2001), Variations of surface air temperature and
726 sea-ice extent in the western Antarctic Peninsula region, *Ann. Glaciol.*, *33*(1), 493–
727 500, doi:10.3189/172756401781818662.

728 Smith, R. C., D. G. Martinson, S. E. Stammerjohn, R. A. Iannuzzi, and K. Ireson (2008),
729 Bellingshausen and western Antarctic Peninsula region: Pigment biomass and sea-
730 ice spatial/temporal distributions and interannual variabilty, *Deep Sea Res. Part II*
731 *Top. Stud. Oceanogr.*, *55*(18-19), 1949–1963, doi:10.1016/j.dsr2.2008.04.027.

732 Stammerjohn, S., R. Massom, D. Rind, and D. Martinson (2012), Regions of rapid sea ice
733 change: An inter-hemispheric seasonal comparison, *Geophys. Res. Lett.*, *39*(6),
734 doi:10.1029/2012GL050874.

735 Stammerjohn, S. E., D. G. Martinson, R. C. Smith, and R. a. Iannuzzi (2008a), Sea ice in
736 the western Antarctic Peninsula region: Spatio-temporal variability from ecological
737 and climate change perspectives, *Deep Sea Res. Part II Top. Stud. Oceanogr.*,
738 *55*(18-19), 2041–2058, doi:10.1016/j.dsr2.2008.04.026.

739 Stammerjohn, S. E., D. G. Martinson, R. C. Smith, X. Yuan, and D. Rind (2008b),
740 Trends in Antarctic annual sea ice retreat and advance and their relation to El Niño–
741 Southern Oscillation and Southern Annular Mode variability, *J. Geophys. Res.*,
742 *113*(C3), C03S90, doi:10.1029/2007JC004269.

743 Steinacher, M., F. Joos, T. L. Frölicher, G.-K. Plattner, and S. C. Doney (2009),
744 Imminent ocean acidification in the Arctic projected with the NCAR global coupled
745 carbon cycle-climate model, *Biogeosciences*, *6*(4), 515–533, doi:10.5194/bg-6-515-
746 2009.

747 Stone, M. (1974), Cross-validatory choice and assessment of statistical predictions, *J. R.*
748 *Stat. Soc. (Series B)*, 111–147.

749 Suess, E., W. Balzer, K. F. Hesse, P. J. Müller, C. A. Ungerer, and G. Wefer (1982),
750 Calcium carbonate hexahydrate from organic-rich sediments of the antarctic shelf:
751 precursors of glendonites., *Science*, *216*, 1128–1131,
752 doi:10.1126/science.216.4550.1128.

753 Sweeney, C., E. Gloor, A. R. Jacobson, R. M. Key, G. McKinley, J. L. Sarmiento, and R.
754 Wanninkhof (2007), Constraining global air-sea gas exchange for CO_2 with recent

755 bomb 14 C measurements, *Global Biogeochem. Cycles*, *21*(2),
756 doi:10.1029/2006GB002784.

757 Takahashi, T., Sutherland, S. C., Wanninkhof, R., Sweeney, C., Feely, R. A., Chipman,
758 D. W., Hales, B., Friederich, G., Chavez, F., Watson, A., Bakker, D. C. E.,
759 Schuster, U., Metzl, N., Yoshikawa-Inoue, H., Ishii, M., Midorikawa, T., Nojiri,
760 Y., Sabine, C., Olafsson, J., Arnarson, T. S., Tilbrook, B., Johannessen, T., Olsen,
761 A., Bellerby, R., Körtzinger, A., Steinhoff, T., Hoppema, M., de Baar, H. J. W.,
762 Wong, C. S., Delille, B. and Bates, N. R. (2009), Climatological mean and
763 decadal changes in surface ocean pCO_2, and net sea-air CO_2 flux over the global
764 oceans. Deep-Sea Res. II, 56, 554-577. doi: 10.1016/j.dsr2.2008.12.009.

765 Takahashi, T., S. C. Sutherland, D. W. Chipman, J. G. Goddard, C. Ho, T. Newberger, C.
766 Sweeney, and D. R. Munro (2014), Climatological distributions of pH, pCO_2, total
767 CO_2, alkalinity, and $CaCO_3$ saturation in the global surface ocean, and temporal
768 changes at selected locations, *Mar. Chem.*, *164*, 95–125,
769 doi:10.1016/j.marchem.2014.06.004.

770 Takahashi, T., S.C. Sutherland and A. Kozyr (2015), Global Ocean Surface Water Partial
771 Pressure of CO_2 Database: Measurements Performed During 1957-2014 (Version
772 2014). ORNL/CDIAC-161, NDP-088(V2014). Carbon Dioxide Information
773 Analysis Center, Oak Ridge National Laboratory, U.S. Department of Energy,
774 Oak Ridge, Tennessee, doi: 10.3334/CDIAC/OTG.NDP088(V2014).

775 Tortell, P. D., E. C. Asher, H. W. Ducklow, J. A. L. Goldman, J. W. H. Dacey, J. J.
776 Grzymski, J. N. Young, S. A. Kranz, K. S. Bernard, and F. M. M. Morel (2014),
777 Geophysical Research Letters, 6803–6810, doi:10.1002/2014GL061266.Received.

778 Vernet, M., D. Martinson, R. Iannuzzi, S. Stammerjohn, W. Kozlowski, K. Sines, R.
779 Smith, and I. Garibotti (2008), Primary production within the sea-ice zone west of
780 the Antarctic Peninsula: I—Sea ice, summer mixed layer, and irradiance, *Deep Sea*
781 *Res. Part II Top. Stud. Oceanogr.*, *55*(18-19), 2068–2085,
782 doi:10.1016/j.dsr2.2008.05.021.

783 Wang, X., G.-P. Yang, D. López, G. Ferreyra, K. Lemarchand, and H. Xie (2009), Late
784 autumn to spring changes in the inorganic and organic carbon dissolved in the water
785 column at Scholaert Channel, West Antarctica, *Antarct. Sci.*, *22*(02), 145,
786 doi:10.1017/S0954102009990666.

787 Weber, T. S., and C. Deutsch (2010), Ocean nutrient ratios governed by plankton
788 biogeography., *Nature*, *467*(7315), 550–4, doi:10.1038/nature09403.

789 Weiss, R. (1974), Carbon dioxide in water and seawater: the solubility of a non-ideal gas,
790 *Mar. Chem.*, *2*(3), 203–215, doi:10.1016/0304-4203(74)90015-2.

Wolf-Gladrow, D. A., R. E. Zeebe, C. Klaas, A. Körtzinger, and A. G. Dickson (2007), Total alkalinity: The explicit conservative expression and its application to biogeochemical processes, *Mar. Chem.*, *106*, 287–300, doi:10.1016/j.marchem.2007.01.006.

Yamamoto-Kawai, M., F. A McLaughlin, E. C. Carmack, S. Nishino, and K. Shimada (2009a), Aragonite undersaturation in the Arctic Ocean: effects of ocean acidification and sea ice melt., *Science*, *326*(5956), 1098–100, doi:10.1126/science.1174190.

Yuan, X. (2004), ENSO-related impacts on Antarctic sea ice: a synthesis of phenomenon and mechanisms, *Antarct. Sci.*, *16*(4), 415–425, doi:10.1017/S0954102004002238.

Yuan, X., and D. G. Martinson (2001), The Antarctic dipole and its predictability, *Geophys. Res. Lett.*, *28*(18), 3609–3612, doi:10.1029/2001GL012969.

Figures.

Figure 1. Map of the Western Antarctic Peninsula (WAP) and study area of the Palmer Antarctica Long Term Ecological Research (PAL-LTER) project. The red box shows the main study grid that has been sampled for inorganic carbon chemistry since 1993, and is defined in this study as the central sub-region. The black squares indicate the stations (20 km apart) arranged in onshore to offshore lines spaced 100 km apart along the peninsula. The inorganic carbon measurements from stations south of the central sub-region were only added in 2009. The central sub-region also contains surface underway pCO_2 observations that were used in the trend analysis (Section 3.5). P: Palmer Station on Anvers Island; A: Adelaide Island; and MB: Marguerite Bay.

Figure 2. Comparison of deep-water (off shelf) dissolved inorganic carbon (DIC, μmol kg^{-1}) and total alkalinity (TA, μmol kg^{-1}) data from Palmer Station Long Term Ecological Research (PAL-LTER) with other available cruise data. a) Station locations, b) DIC and c) TA depth profiles from PAL-LTER cruises (1998-2012), World Ocean Circulation Experiment (WOCE) and Ocean – Variability, Predictability, and Change (CLIVAR) cruises along parts of sections A21 (2006, 2009) and S4P (1992, 2011). The directly measured parameters are listed in the parentheses and were used to calculate TA if not directly measured.

Figure 3. Depth profiles of aragonite saturation state (Ω_{arag}) for the years 1993 through 2012. The aragonite saturation horizon for each year is located where the profile crosses the black line ($\Omega_{arag} = 1.0$).

Figure 4. Maps of summertime averages of surface a) pCO_2, b) pHT, c) aragonite saturation state (Ω_{arag}), d) total alkalinity (TA, μmol kg^{-1}), e) salinity, f) dissolved inorganic carbon (DIC, μmol kg^{-1}), and g) salinity-normalized DIC (sDIC, μmol kg^{-1}) across years with available DIC and TA measurements (1993-1999, 2001-2002, and 2005-2012). Salinity-normalized PO_4^{3-} (s PO_4^{3-}, μmol kg^{-1}) and salinity normalized NO_3^- (s NO_3^-, μmol kg^{-1}) were avaeraged across 1993-1996, 1999, and 2001-2012. Averages

836 are only shown for regions where samples were taken in five or more years. Occupied
837 stations are shown by black dots.
838
839 **Figure 5.** Scatter plots of dissolved inorganic carbon (DIC, μmol kg^{-1}) illustrated as
840 diamonds and total alkalinity (TA, μmol kg^{-1}) illustrated as dots as a function of salinity.
841 The data points are color coded by the aragonite saturation state (Ω_{arag}). The solid lines
842 illustrate the dilution lines using S = 34.7, TA = 2350 μmol kg^{-1}, and DIC = 2253 μmol
843 kg^{-1} as end members for UCDW, and S = 0, TA = 300 μmol kg^{-1}, and DIC = 300 μmol
844 kg^{-1} as end members for melt water [*Yamamoto-Kawai et al.*, 2009]. WW = Winter water
845 (T <= -1.2 C°; 33.85 =< S =< 34.13), UCDW = Upper Circumpolar Deep Water (1.7 C°
846 => T =< 2.13 C°; 34.54 =< S =< 34.75) following [*Martinson et al.*, 2008].
847
848 **Figure 6.** Salinity-normalized total alkalinity (sTA, μmol kg^{-1}) as a function of salinity-
849 normalized dissolved inorganic carbon (sDIC, μmol kg^{-1}) for waters shallower than the
850 Upper Circumpolar Deep Water (UCDW, black circles). A linear fit between sTA and
851 sDIC is shown by the black solid line. The dotted black lines indicate 2σ for estimated
852 measurement precision of σ = +/- 5 μmol kg^{-1}. The blue line illustrates the trend if sTA
853 and sDIC of the winter water (WW) were only influenced by photosynthesis (1:-6.2).
854 Grey dots represent sTA as a function of sDIC corrected for gas exchange in the waters
855 above the WW, and the linear fits with the estimated measurement precision are the grey
856 solid and dashed lines respectively. WW: T <= -1.2 C°; 33.85 =< S =< 34.13, UCSW: 1.7
857 C°=> T =< 2.13 C°; 34.54 =< S =< 34.75, following [*Martinson et al.*, 2008].
858
859 **Figure 7.** Plot of salinity-normalized nutrients and dissolved inorganic carbon (sDIC,
860 μmol kg^{-1}), a) sPO_4^{3-} (μmol kg^{-1}) versus sNO_3^- (μmol kg^{-1}), b) sPO_4^{3-} versus sDIC, and c)
861 sNO_3^- versus sDIC. Observations within the mixed layer (~ depth < 50 m) are illustrated
862 by black circles. The light grey dots in b) and c) show sDIC corrected for gas exchange as
863 a function of sPO_4^{3-} and sNO_3^-, respectively. A linear fit is represented by the solid black
864 line for the mixed layer, by the solid grey line for all data, and by the light grey line for
865 the gas-exchange corrected sDIC in b) and c). The dashed black lines are the nutrient

drawdown lines using the corresponding Redfield ratio and data from the Upper Circumpolar Deep Water (UCDW) as end-members.

Figure 8. Seasonal variability of inorganic carbon system. Relative frequency distribution of a) measured underway surface partial pressure pCO_2 (µatm), b) predicted surface total alkalinity (TA, µmol kg^{-1}) from underway salinity, and c) predicted surface aragonite saturation state (Ω_{arag}) in summer (red), fall (orange), winter (blue), and spring (yellow). The x-axis represents the range of Ω_{arag}, TA, and pCO_2 with a relative frequency distribution >= 0.0001.

Table 1. Comparison of Lamont-Doherty Earth Observatory of Columbia University (LDEO) underway pCO_2 (µatm) data [*Takahashi et al*., 2015] with the pCO_2 (µatm) derived from PAL-LTER discrete surface samples over the Palmer-Long Term Ecological Research (PAL-LTER) sampling grid. The PAL-LTER discrete pCO_2 sample values were computed using the dissolved inorganic carbon (DIC, µmol kg^{-1}) and total alkalinity (TA, µmol kg^{-1}). The analysis is based on the data after removing outliers as explained in the text.

		Mean (std)	r	Slope	Intercept	n
2005	LDEO	293 (79)	0.94	1.05 (±0.06)	-45.7 (±17.0)	49
	PAL-LTER	322 (75)				
2006	LDEO	248 (46)	0.90	0.95 (±0.06)	13.2 (±15)	55
	PAL-LTER	248 (48)				
2007	LDEO	261 (61)	0.87	1.04 (±0.08)	14.7 (±18.5)	60
	PAL-LTER	237 (59)				
2008	LDEO	340 (28)	0.53	0.61 (±0.14)	158 (±42.5)	48
	PAL-LTER	299 (37)				
2009	LDEO	318 (24)	0.58	0.47 (±0.13)	179 (±37.9)	27
	PAL-LTER	292 (37)				
2010	LDEO	327 (35)	0.54	1.62 (±0.57)	-167 (±174)	20
	PAL-LTER	305 (27)				
2011	LDEO	226 (98)	0.93	0.97 (±0.9)	0.60 (±21.4)	21
	PAL-LTER	233 (101)				
2012	LDEO	354 (36)	0.46	1.44 (±0.63)	-47.7 (±172)	21
	PAL-LTER	279 (30)				
All	LDEO	290 (69)	0.82	1.08 (±0.04)	-5.57 (±12.2)	300
	PAL-LTER	275 (65)				

884 **Table 2.** Mean annual trend (1993-2012) of Palmer-Long Term Ecological Research
885 (PAL-LTER) surface (depth < 5 m) carbonate chemistry and hydrography from the
886 Western Antarctic Peninsula (central sub-region). Regression statistics include the mean
887 annual rate (yr^{-1}), standard error (SE), number of measurements (NM), number of years
888 (NY), r-square, and p-value for aragonite saturation state (Ω_{arag}), pHT, dissolved
889 inorganic carbon (DIC, μmol kg^{-1}), total alkalinity (TA, μmol kg^{-1}), temperature (°C), and
890 salinity. Trends with a p-value < 0.05 are statistically significant at the 95 % confidence
891 level (values bolded). Points that were outliers at 95 % probability level were excluded
892 (o).
893

Parameter	Rate (yr^{-1}) ± SE	NM(o)	NY	r^2	p-value
	Surface (< 5 m depth)				
Ω_{arag}	0.001 ± 0.01	892(17)	18	0.04	0.9127
pHT	0.002 ± 0.002	892(8)	18	0.03	0.2784
DIC (μmol kg^{-1})	-0.18 ± 1.03	907(0)	18	0.00	0.8677
TA (μmol kg^{-1})	0.58 ± 0.63	907(0)	18	0.05	0.3681
Temperature (°C)	-0.01 ± 0.02	1076(8)	20	0.01	0.4629
Salinity	0.01 ± 0.01	1060(8)	20	0.12	0.1349

894

895 **Table 3.** Trend analysis (1999-2013) of Lamont-Doherty Earth Observatory of Columbia
896 University (LDEO) surface continuous underway pCO_2 (μatm), salinity and temperature
897 (°C) measurements from within the central sub-region of the Palmer-Long Term
898 Ecological Research (PAL-LTER) sampling grid (Figure 1, red box). Regression
899 statistics include mean rate, standard error (SE), number of measurements (NM), number
900 of years (NY), r-square, and p-value. Trends with a p-value < 0.05 would be considered
901 statistically significant at the 95 % confidence level.

Parameter	Season	Rate ± SE	NM	NY	r^2	p-value
		Central sub-region				
pCO_2 (μatm yr^{-1})	Summer	1.45 ± 2.97	94774	12	0.01	0.6361
	Fall	1.90 ± 0.95	42655	14	0.26	0.0685
	Winter	0.43 ± 0.77	26314	11	0.04	0.6304
	Spring	1.22 ± 2.72	14813	9	0.03	0.6678
Temperature (°C yr^{-1})	Summer	0.03 ± 0.05	94774	13	0.03	0.5515
	Fall	0.00 ± 0.05	42655	14	0.01	0.9279
	Winter	0.00 ± 0.04	26314	13	0.00	0.9262
	Spring	0.01 ± 0.03	14813	9	0.04	0.8598
Salinity (yr^{-1})	Summer	-0.02 ± 0.02	53713	12	0.10	0.3294
	Fall	0.02 ± 0.01	55823	13	0.14	0.0988
	Winter	-0.01 ± 0.01	28063	10	0.01	0.6631
	Spring	-0.01 ± 0.01	53713	11	0.05	0.1422

902

903 Figure 1

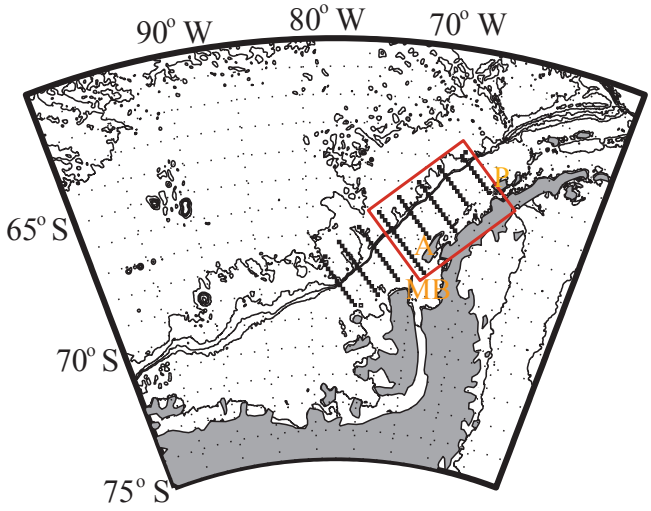

904
905
906

907 Figure 2
908

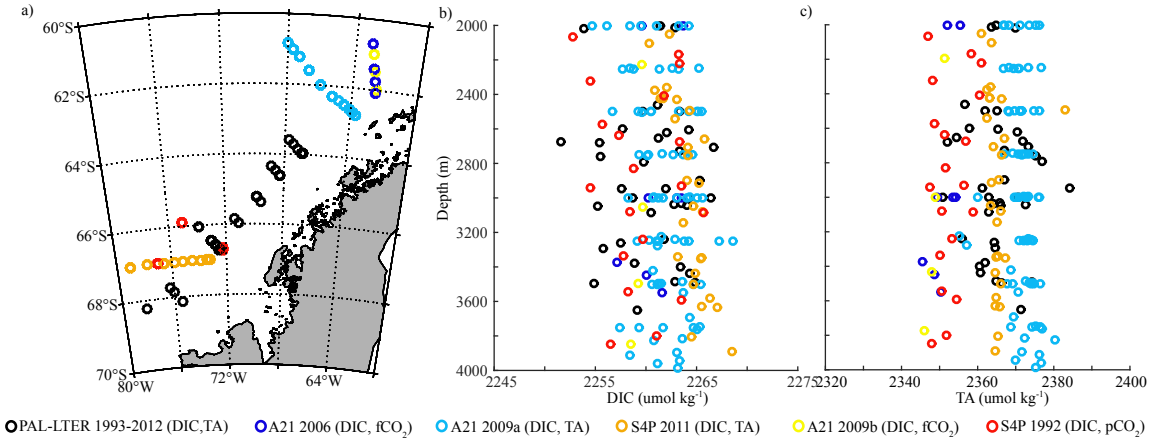

909
910

911 Figure 3

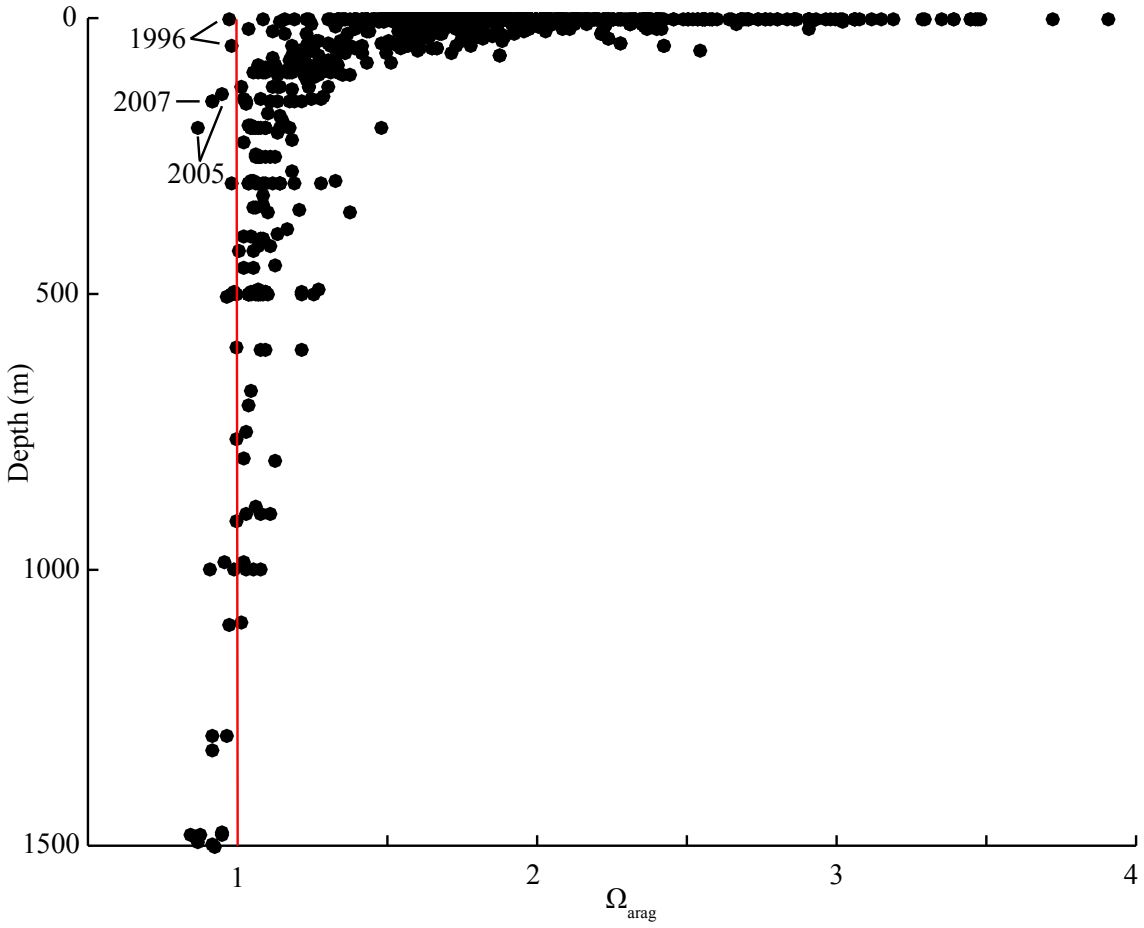

912

913 Figure 4

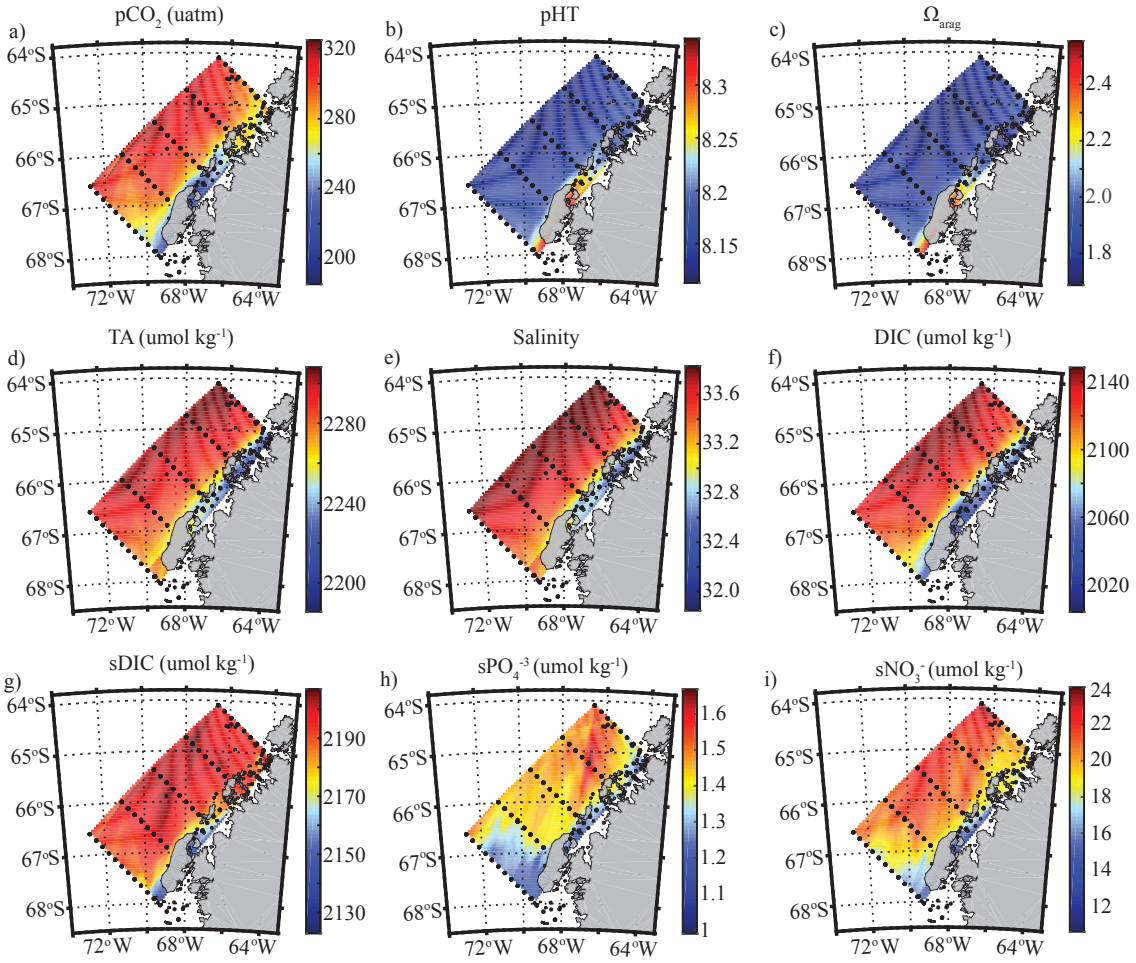

914
915

916
917 Figure 5:
918

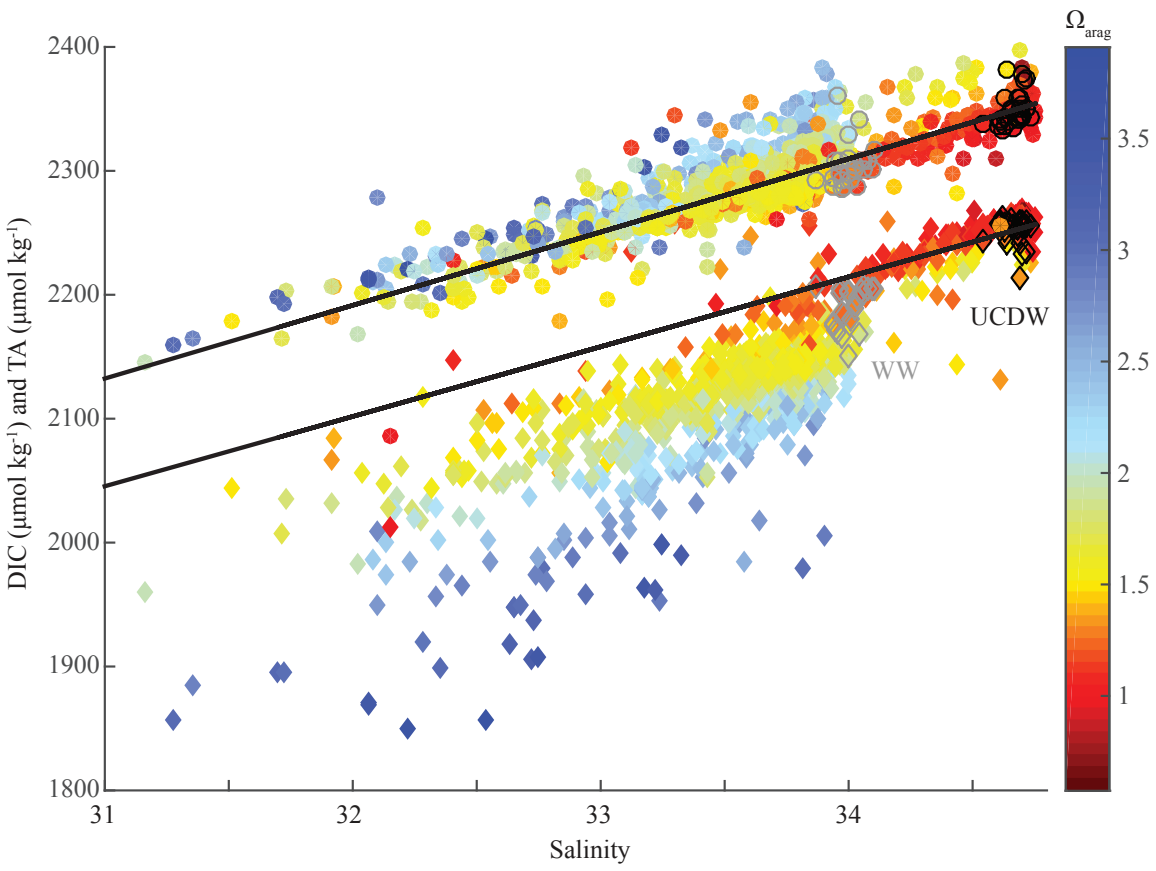

919

920 Figure 6

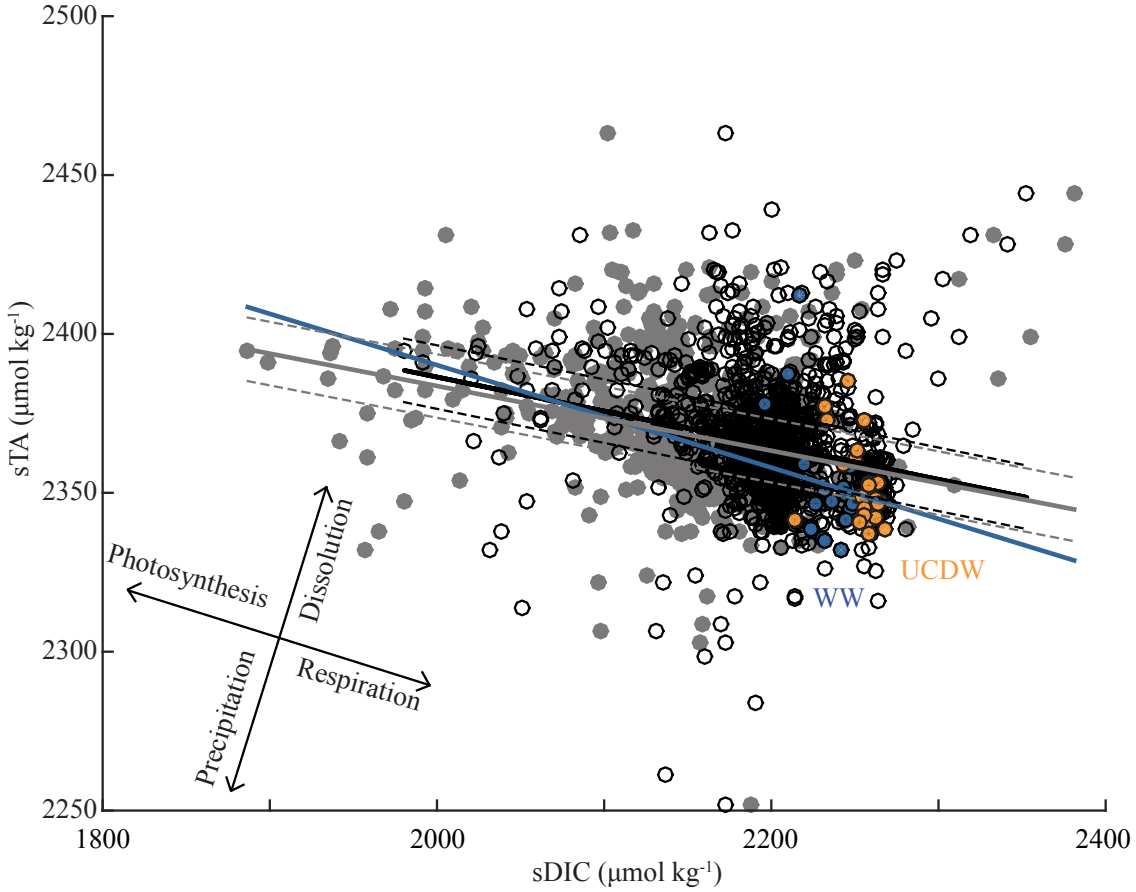

921

922 Figure 7

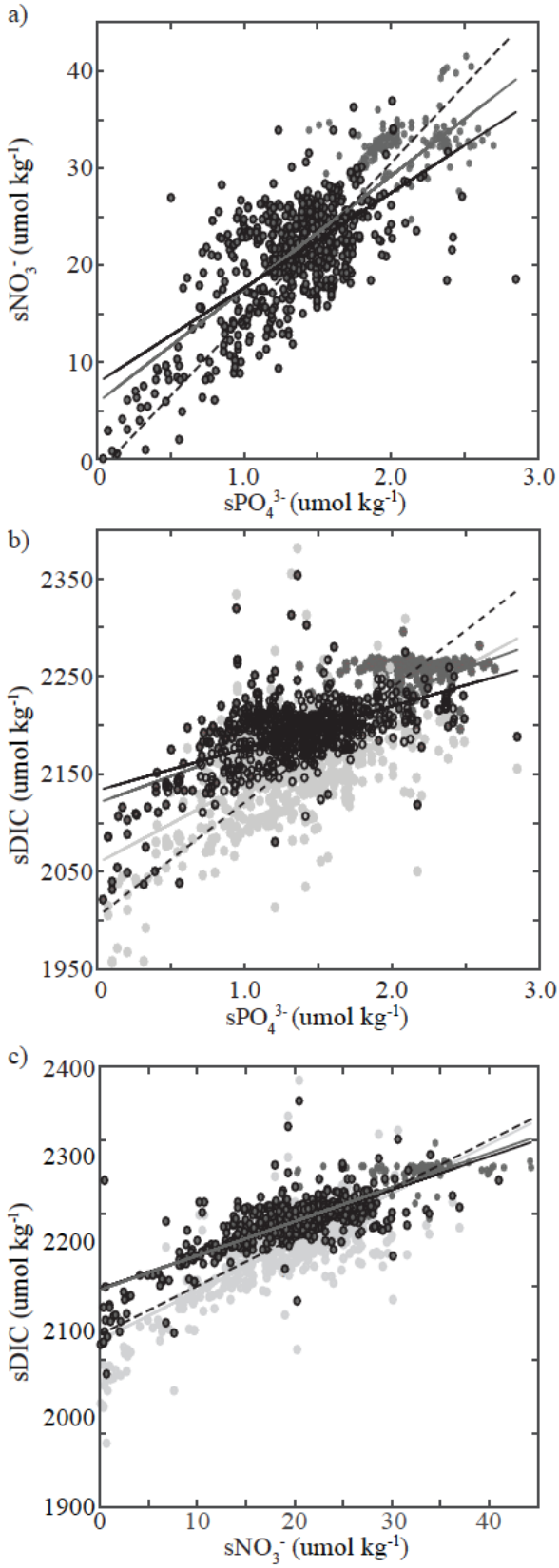

923

924 Figure 8
925

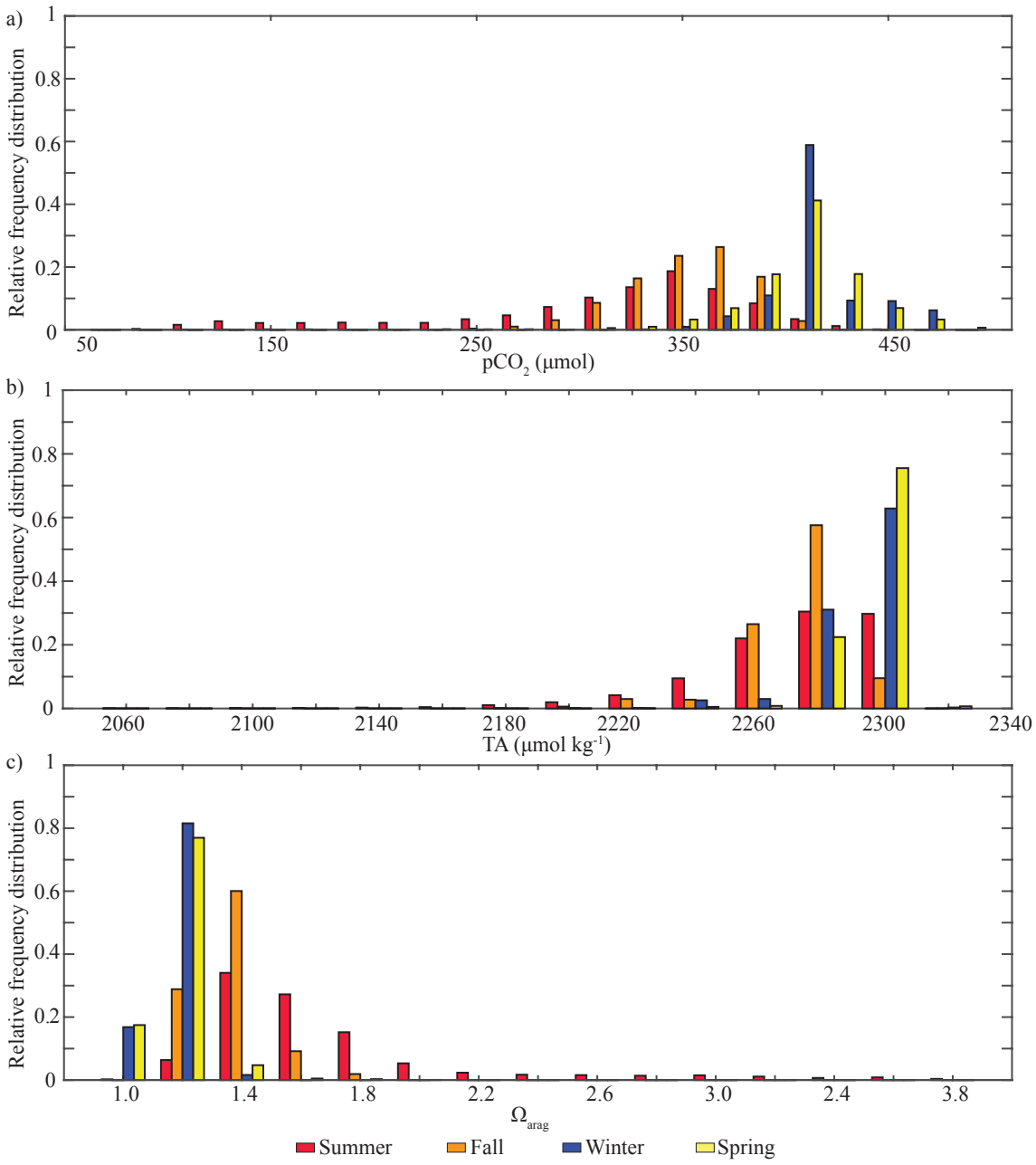

926

927

928 Appendix

929

930 **Figure A1.**
931 Comparison of Lamont-Doherty Earth Observatory of Columbia University (LDEO)
932 continuous underway pCO_2 (µatm) over the Palmer-Long Term Ecological Research
933 (PAL-LTER) sampling grid (Takahashi et al., 2015) with pCO_2 (µatm) derived from
934 PAL-LTER dissolved inorganic carbon (DIC, µmol kg^{-1}) and total alkalinity (TA, µmol
935 kg^{-1}) from discrete samples taken during the same cruise (2005-2012). PAL-LTER pCO_2
936 outliers that underestimate/overestimate pCO_2 relative to the underway observations by
937 more than 150 µatm were removed. The two data sets were spatially matched, with a 1
938 km distance threshold. See Table 1 for statistics.
939

940 **Figure A2.**
941 Evaluation of total alkalinity (TA) algorithm. a) Measured TA as a function of salinity
942 and temperature (color), b) measured TA vs. predicted TA, and c) residuals vs. salinity.
943

944 **Figure A3**
945 Scatterplots of depth and inorganic carbon chemistry superimposed on potential
946 temperature-salinity diagrams. Shown in color are a) depth, b) dissolved inorganic carbon
947 (DIC, µmol kg^{-1}), c) total alkalinity (TA, µmol kg^{-1}), and d) aragonite saturation state
948 (Ω_{arag}). The bold black line illustrates the freezing point as a function of temperature and
949 salinity. Grey lines mark densities. Water masses are indicated and labeled in a): WW =
950 Winter Water, AASW = Antarctic Surface Water in summer, ACC-core UCDW =
951 Antarctic Circumpolar Current-core Upper Circumpolar Deep Water, DW = local Deep
952 Water end member, following *Martinson et al.,* [2008].
953
954

955 Figure A1
956

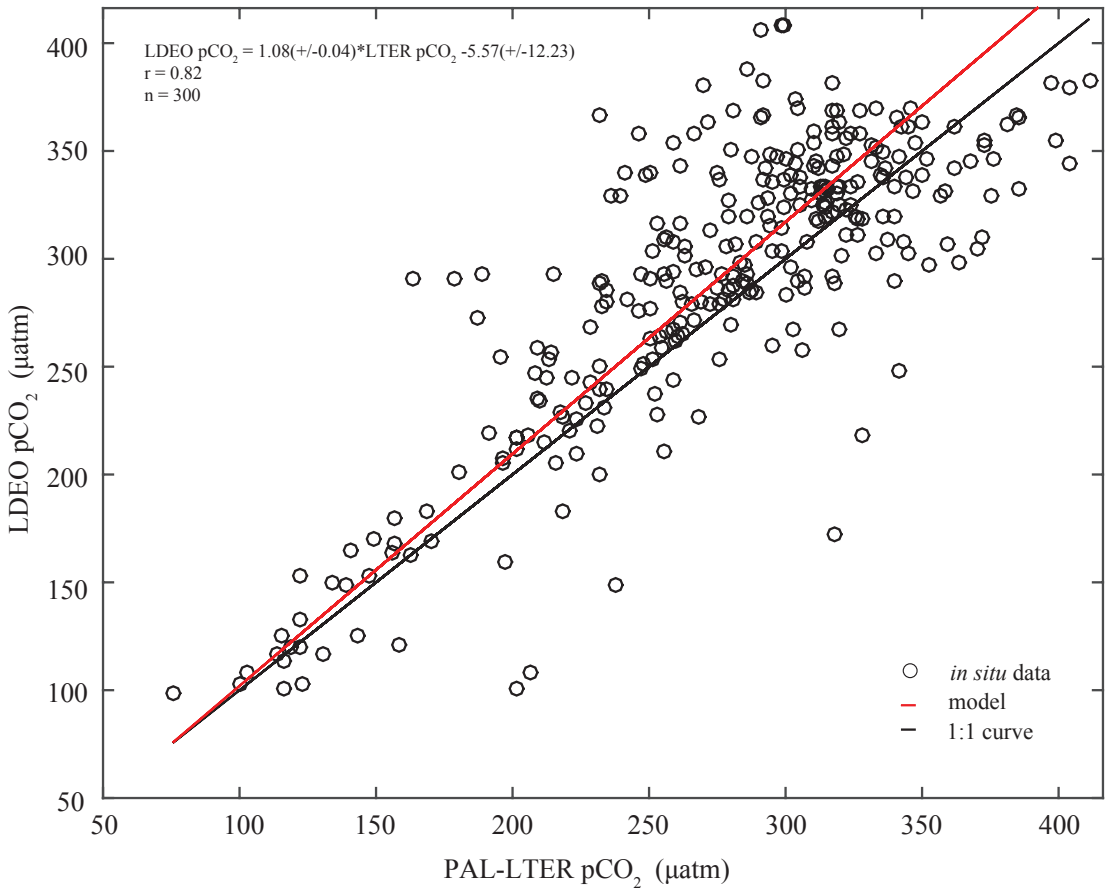

957
958

959 Figure A2

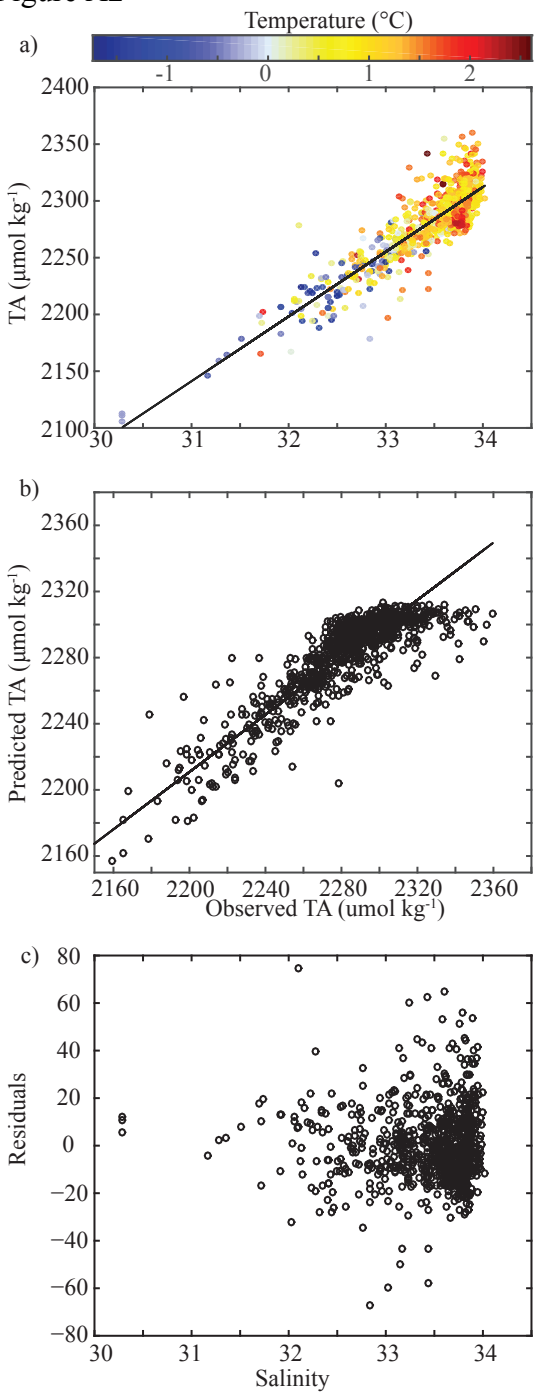

960
961

962 Figure A3
963

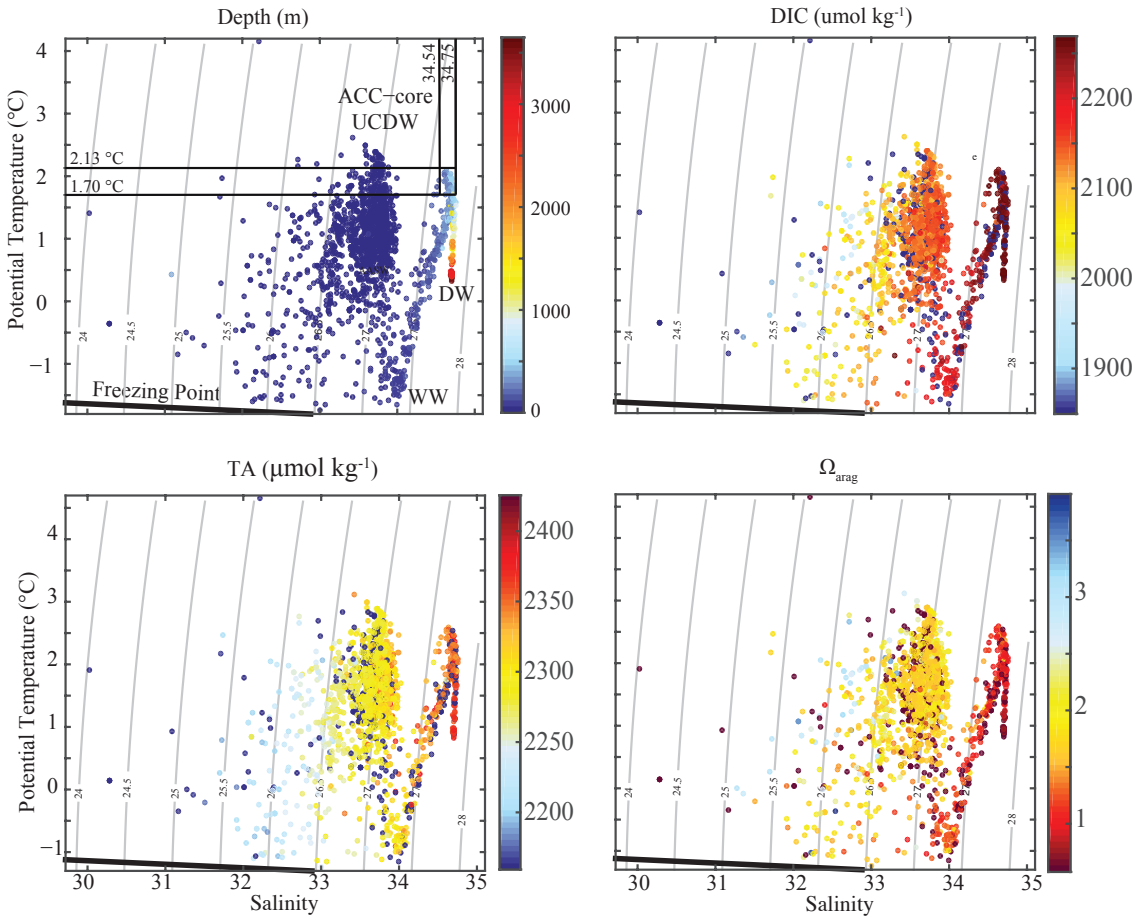

964
965

966